Convolutional Beamspace for Linear Arrays

Po-Chih Chen, *Student Member, IEEE*, and P. P. Vaidyanathan, *Life Fellow, IEEE*

***Abstract*—A new beamspace method for array processing, called convolutional beamspace (CBS), is proposed. It enjoys the advantages of classical beamspace such as lower computational complexity, increased parallelism of subband processing, and improved resolution threshold for DOA estimation. But unlike classical beamspace methods, it allows root-MUSIC and ESPRIT to be performed directly for ULAs without additional preparation since the Vandermonde structure and the shift-invariance are preserved under the CBS transformation. The method produces more accurate DOA estimates than classical beamspace, and for correlated sources, better estimates than element-space. The method also generalizes to sparse arrays by effective use of the difference coarray. For this, the autocorrelation evaluated on the ULA portion of the coarray is filtered appropriately to produce the coarray CBS. It is also shown how CBS can be used in the context of sparse signal representation with dictionaries, where the dictionaries have columns that resemble steering vectors at a dense grid of frequencies. Again CBS processing with dictionaries offers better resolution, accuracy, and lower computational complexity. As only the filter responses at discrete frequencies on the dictionary grid are relevant, the problem of designing discrete-frequency FIR filters is also addressed.**

***Index Terms*—Convolutional beamspace, DOA estimation, sparse arrays, dictionaries, root-MUSIC, ESPRIT.**

I. Introduction

In ARRAY signal processing, the use of beamforming prior to high-resolution estimation of directions of arrival (DOA), referred to as *beamspace* processing, is well-known in the literature [1]–[5], and continues to be of current research interest [6]–[8]. Given an N-sensor array with output $\mathbf{x} \in \mathbb{C}^N$, the idea of beamspace is to compute a transformation $\mathbf{y} = \mathbf{T}\mathbf{x} \in \mathbb{C}^B$, where $B < N$, and estimate the DOAs using $\mathbf{y}$. For example, the covariance of $\mathbf{y}$ can be estimated from its snapshots, and its signal and noise eigenspaces are analyzed to perform DOA estimation as in MUSIC [9], root-MUSIC [10], or ESPRIT [11].

One of the major advantages of beamspace processing is complexity reduction. Due to dimensionality reduction ($B < N$), the $B \times B$ covariance of $\mathbf{y}$ has smaller size than that of $\mathbf{x}$. So the complexity of the eigenspace computation $O(B^3)$, is much smaller than $O(N^3)$, which is the complexity when using *element-space* ($\mathbf{T} = \mathbf{I}$) directly. If $\mathbf{T}$ is carefully chosen, then the DOAs which fall outside a chosen subband in $[-\pi/2, \pi/2)$ are attenuated by $\mathbf{T}$, so there are typically much fewer DOAs represented by $\mathbf{y}$, compared to $\mathbf{x}$. One often uses a bank of transformations $\{\mathbf{T}_i\}$, which can be operated *in parallel*, to cover all DOAs in $[-\pi/2, \pi/2)$.

Besides low computation and parallelism, there are other advantages for beamspace. Beamspace methods tend to have smaller SNR threshold for resolution of closely spaced sources [5], [12], [13]. Beamspace estimates typically have smaller bias (and about the same mean square error) when compared with element-space estimates [14].

However, to successfully perform root-MUSIC after the classical beamspace transformation, one has to take elaborate steps [14]. Specifically, rows of $\mathbf{T}$ are chosen to be columns of the DFT matrix, producing beams exhibiting common out-of-band nulls. These nulls result in spurious roots outside the subband, independent of the true in-band DOAs. The spurious roots are factored out to reduce the degree of the polynomial to be rooted so as to lower the complexity. Moreover, this method suffers from numerical sensitivity issues [14] for even moderately large array size N, such as $N = 48$. Similarly, classical beamspace transformation also compromises the shift-invariance structure required by ESPRIT. One has to choose $\mathbf{T}$ to have the same shift-invariance structure so that the lost shift-invariance structure can be restored with a modified ESPRIT algorithm [15].

A. Contributions of This Paper

In this paper we introduce a new approach called the *convolutional beamspace (CBS)* approach. It enjoys the advantages of classical beamspace such as lower computational complexity, increased parallelism of subband processing, and improved resolution threshold for DOA estimation. Furthermore, unlike classical beamspace methods, it allows root-MUSIC and ESPRIT to be performed directly for uniform linear arrays (ULAs) without additional preparation since the Vandermonde structure and the shift-invariance are preserved under the CBS transformation. The computational benefits of the proposed methods are quantified and demonstrated throughout.

Unlike classical beamspace, CBS is based on the use of filtering with a finite-impulse-response (FIR) filter $H(z)$ followed by uniform downsampling (decimation) by an appropriate integer M. For large arrays, which are becoming increasingly important [16], [17], the filter can be proportionately longer, offering very effective attenuation of out-of-band DOAs. CBS produces more accurate DOA estimates than classical beamspace, and for correlated sources it often produces better estimates than element-space as well. Crucial to the CBS method is the extraction of a steady-state component from the convolutional layer, as we shall see.

We also provide an error analysis of the CBS method, based on error analysis for MUSIC [18] (Section II-F). For uncorrelated

Manuscript received February 21, 2020; revised June 19, 2020 and August 21, 2020; accepted August 31, 2020. Date of publication September 4, 2020; date of current version September 29, 2020. The associate editor coordinating the review of this manuscript and approving it for publication was Dr. David Ramirez. This work was supported in parts by the ONR under Grant N00014-18-1-2390, the NSF under Grant CCF-1712633, and the California Institute of Technology. *(Corresponding author: Po-Chih Chen.)*

The authors are with the Department of Electrical Engineering, California Institute of Technology, Pasadena, CA 91125 USA (e-mail: pochih@caltech.edu; ppvnath@systems.caltech.edu).

Digital Object Identifier 10.1109/TSP.2020.3021670

sources, the error variance of CBS estimates is shown to be close to that of the element-space. However, for correlated sources, CBS can be significantly better. These conclusions are also verified with simulations.

The CBS method in Section II is for the ULA, but we show in Section III that it can be extended to sparse arrays by appealing to the difference coarray of the original array. Difference coarrays of sparse arrays such as the MRA [19], nested array [20], coprime array [21], and their generalizations [22], [23] contain a large ULA segment. Since the autocorrelation of measured data can be estimated for all lags on the coarray, one can perform FIR filtering of the correlation supported on the ULA part of the coarray to produce a convenient CBS. This coarray CBS offers great computational reduction. The advantage of sparse arrays, namely the ability to identify $O(N^2)$ uncorrelated sources with N sensors [20], [21], can be harnessed even while taking advantage of the benefits of the CBS transformation.

Finally we also show how CBS ideas can be used in the context of sparse signal representation with dictionaries. The use of sparse representation techniques for DOA estimation has been studied in [24] where a dictionary of steering vectors (corresponding to a dense grid of potential DOAs) is used to represent the array output. The sparse solution to this representation problem reveals the DOAs. We show how this problem can be simplified computationally by use of CBS techniques. Besides its significant computational advantage, the method also produces more accurate DOA estimates. Since only the filter responses $H(e^{j\omega_k})$ at the discrete frequencies on the dictionary grid are relevant at the convolutional layer, we also address the interesting problem of designing discrete-frequency FIR filters for CBS dictionaries. Eigen-based methods such as MUSIC and dictionary-based sparse recovery methods are both well-known DOA estimation algorithms in the literature. The main goal of this paper is to show that CBS can be applied to both methods, and to coarray based methods.

B. Related Past Work

The use of convolution (digital filtering) prior to frequency estimation for time-domain sum-of-sinusoids was introduced many years ago by Silverstein, et al. [25], and studied in detail in [26]. But these methods, and many of the details in [26], are not directly applicable to spatial arrays. The purpose of this paper is to develop the appropriate formulation for spatial arrays, and provide several extensions, such as extensions to coarrays and to dictionary methods.

In [27], an alternating low-rank decomposition (ALRD) approach is proposed. Each row of the beamspace transformation matrix $\mathbf{T}$ contains a basis vector to be optimized. A constrained optimization problem based on Capon's minimum-variance criterion is tackled by alternately solving for the basis vectors and the beamforming weight vector using the recursive least squares (RLS) method. A modified-ALRD (MALRD) scheme [27], where only a single basis vector is used, is also proposed to reduce computational complexity. In the MALRD scheme, the transformation matrix $\mathbf{T}$ is equivalent to doing convolution followed by uniform decimation. However, CBS differs from MALRD in that only CBS uses the idea of digital filtering so that standard filter design methods such as the minimax or equiripple method, the window method, and so on [28], can be applied. Moreover, only CBS exploits the Vandermonde structure of the convolutional steady state so that root-MUSIC and ESPRIT can be applied directly. Also note that MALRD is a special case of the joint iterative optimization (JIO) algorithms [29], [30]. Besides the uniform decimation used in MALRD, non-uniform decimation is also considered in [30]. But to preserve the Vandermonde structure of ULAs so that root-MUSIC and ESPRIT can be readily applied, we always use uniform decimation for CBS. Moreover, we will show by simulation (Fig. 6) that there is no loss of performance in using uniform decimation since it achieves the same error variance as not doing decimation (i.e., keeping all samples) does.

Preliminary versions of the basic ideas in Section II are presented in a conference paper [31].

Paper outline: The basic idea of CBS for ULAs is introduced in Section II, and details of dimension reduction using uniform decimation, noise whitening in the reduced space using Nyquist filter design, and error analysis are also presented. The extension to sparse arrays based on difference coarrays is addressed in Section III. CBS for dictionary-based sparse signal recovery is then discussed in Section IV. Simulations in Secs. II, III, and IV demonstrate the performance of the new method. Section V concludes the paper.

Notations: Boldfaced capital letters denote matrices and boldfaced lowercase letters are reserved for column vectors. We use $(\cdot)^*$, $(\cdot)^T$, and $(\cdot)^H$ to denote complex conjugate, transpose, and conjugate transpose, respectively. The identity matrix is denoted by $\mathbf{I}$, and $\mathrm{E}[\cdot]$ is the expectation operator.

II. Convolutional Beamspace for ULAs

We consider an N-sensor ULA with sensor spacing $\lambda/2$, and monochromatic plane waves of wavelength λ arriving from D directions. The array output equation is

$$\mathbf{x} = \mathbf{A}\mathbf{c} + \mathbf{e}, \tag{1}$$

where $\mathbf{c}$ contains source amplitudes c_i, $\mathbf{e}$ contains additive noise terms, and $\mathbf{A} = [\mathbf{a}_N(\omega_1)\ \mathbf{a}_N(\omega_2) \cdots \mathbf{a}_N(\omega_D)]$ with $\mathbf{a}_N(\omega) = [1\ e^{j\omega}\ e^{j2\omega}\ \cdots\ e^{j(N-1)\omega}]^T$, so that $\mathbf{A}$ is a Vandermonde matrix. Here $\omega = \pi \sin\theta$, with DOA $\theta \in [-\pi/2, \pi/2)$ measured from the normal to the line of array. We assume $\mathrm{E}[\mathbf{c}] = \mathbf{0}$, $\mathrm{E}[\mathbf{e}] = \mathbf{0}$, $\mathrm{E}[\mathbf{e}\mathbf{e}^H] = \sigma_e^2\mathbf{I}$, and $\mathrm{E}[\mathbf{c}\mathbf{e}^H] = \mathbf{0}$.

The main results of this section are as follows. In Section II-A, we show that the convolutional steady state of the CBS output bears the same structure as the ULA output (1), as shown in (6). In Section II-B, we show how to use uniform decimation to reduce computational complexity. The decimated output (10) still has the Vandermonde structure of the ULA output (1). Hence, root-MUSIC and ESPRIT can be directly applied to the decimated covariance (15) without further adjustment, as explained in Section II-C. In Section II-D, it is shown that by choosing the filter used in CBS to be a spectral factor of Nyquist filters as in (21), we can whiten the noise term after decimation. Then, the computational complexity of CBS is compared to various methods in the literature in Section II-E, and a brief error analysis is given in Section II-F. Finally, simulations are presented in Section II-G.

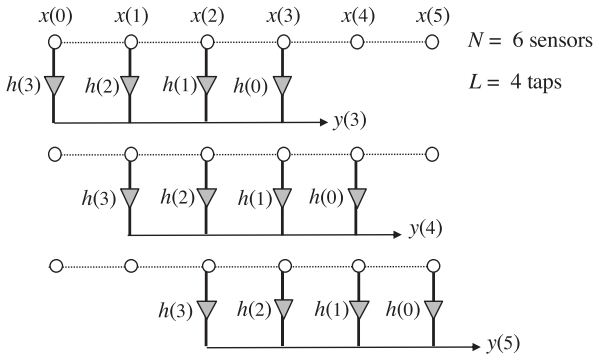

Fig. 1. The steady state CBS signal $\mathbf{y} = [y(3)\ y(4)\ y(5)]^T$ generated by sliding the weights $h(k)$ over the sensors.

A. The Convolutional Steady State

Let $x(n), 0 \le n \le N-1$ be the output of the N-sensor ULA. We convolve this sequence with an FIR filter with transfer function $H(z) = \sum_{n=0}^{L-1} h(n) z^{-n}$ with $L < N$ to get the possibly nonzero output samples $y(n), 0 \le n \le N+L-2$. Of these, only

$$y(L-1), y(L), \cdots, y(N-1) \tag{2}$$

involve all the L filter coefficients, and can be considered *steady state* output samples:

$$\mathbf{y} \triangleq \begin{bmatrix} y(L-1) \\ y(L) \\ \vdots \\ y(N-1) \end{bmatrix} = \mathbf{H} \begin{bmatrix} x(0) \\ x(1) \\ \vdots \\ x(N-1) \end{bmatrix} = \mathbf{H}\mathbf{x}, \tag{3}$$

where $\mathbf{H}$ is a $(N-L+1) \times N$ banded Toeplitz matrix:

$$\mathbf{H} = \begin{bmatrix} h(L-1) & \cdots & h(0) & 0 & \cdots & 0 \\ 0 & h(L-1) & \cdots & h(0) & \cdots & 0 \\ \vdots & \vdots & \ddots & \vdots & \ddots & \vdots \\ 0 & 0 & \cdots & h(L-1) & \cdots & h(0) \end{bmatrix}.$$

For example, $y(L-2)$ does not contain $h(L-1)$ (as $x(-1) = 0$) and $y(N)$ does not contain $h(0)$ (as $x(N) = 0$). So these are not part of the steady state output (3). The steady state samples $\mathbf{y}$ are obtained by sliding the reversed weights $h(k)$ from left to right uniformly, as shown in Fig. 1. We call $\mathbf{y}$ the *convolutional beamspace signal.* In contrast, in classical beamspace $\mathbf{y} = \mathbf{T}\mathbf{x}$, $\mathbf{T}$ is a fat $B \times N$ matrix, but without any Toeplitz structure. For instance, a popular choice is to let $\mathbf{T}$ contain B consecutive rows of the $N \times N$ DFT matrix [14]. As we shall see, the banded Toeplitz structure of $\mathbf{H}$ is essential to obtain a Vandermonde structure in $\mathbf{y}$.

Now assume we have a signal arriving from DOA $\bar{\theta}$ so that $x(n) = e^{j\omega n}, 0 \le n \le N-1$ (up to some scale, which we ignore), where $\omega = \pi \sin\bar{\theta}$. Then from the steady state equation (3), ignoring noise, we have

$$\mathbf{y} = e^{j(L-1)\omega} H(e^{j\omega}) \begin{bmatrix} 1 & e^{j\omega} \cdots & e^{j(N-L)\omega} \end{bmatrix}^T, \tag{4}$$

where $H(z) = \sum_{n=0}^{L-1} h(n) z^{-n}$. So the CBS signal $\mathbf{y}$ in response to a single DOA is a *Vandermonde vector* just like the array output vector $\mathbf{x} = \mathbf{a}_N(\omega) = [1\ e^{j\omega}\ e^{j2\omega}\ \cdots\ e^{j(N-1)\omega}]^T$. Moreover, $\mathbf{y}$ is scaled by the filter frequency response $H(e^{j\omega})$. Thus if there are D sources with DOAs ω_k, then since $x(n) = \sum_{k=1}^{D} c_k e^{j\omega_k n}$, we have

$$\mathbf{y} = \sum_{k=1}^{D} c_k e^{j(L-1)\omega_k} H(e^{j\omega_k}) \mathbf{a}_{N-L+1}(\omega_k) + \mathbf{H}\mathbf{e}. \tag{5}$$

The arriving signals with DOAs ω_k are therefore filtered by the response $H(e^{j\omega})$. Thus the array equation (1) is replaced with

$$\mathbf{y} = \mathbf{A}_L \mathbf{d} + \mathbf{H}\mathbf{e} \tag{6}$$

where $\mathbf{A}_L$ is a Vandermonde matrix obtained from $\mathbf{A}$ by keeping the first $N-L+1$ rows, and $\mathbf{d}$ has elements $d_k = c_k e^{j(L-1)\omega_k} H(e^{j\omega_k})$. While the development is valid for any ULA, for large arrays (large N), which are getting more attention recently [16], we can make L large and design a sharp-cutoff filter with good stopband. Assuming signals in the stopband are not too strong so that $\mathbf{y}$ contains only those DOAs that fall in the passband of $H(e^{j\omega})$, we have

$$\mathbf{y} \approx \mathbf{A}_{L,0} \mathbf{d}_0 + \mathbf{H}\mathbf{e}. \tag{7}$$

Here $\mathbf{A}_{L,0}$ has D_0 columns of $\mathbf{A}_L$ corresponding to the D_0 sources that fall in the passband of $H(e^{j\omega})$, and $\mathbf{d}_0$ has the corresponding D_0 rows of $\mathbf{d}$. Fig. 2 shows a typical filter response, with two out of six DOAs falling in the passband. The FIR filter $H(z)$ can be designed by any standard method such as the minimax or equiripple method, the window method, and so on [28]. If the filter does not have sharp cutoff, it is likely that a DOA falls in the transition band, which requires more careful consideration.

Note that we can process the array output $x(n)$ with an entire *filter bank* $H_i(e^{j\omega}), 0 \le i \le M-1$ to cover the full DOA range $0 \le \omega < 2\pi$, as in Fig. 3. The outputs of filters can be processed *in parallel* to estimate all D DOAs. The DOA estimation procedure would be to first estimate the number of DOAs D_0 from $\mathbf{y}$, and identify these D_0 DOAs using standard methods. Since the filter output $\mathbf{y}$ is represented in terms of the Vandermonde matrix $\mathbf{A}_L$ just like the original array output $\mathbf{x}$, we can use root-MUSIC or ESPRIT without any further adjustment or processing to the data. This is an advantage of the proposed CBS method compared to classical beamspace methods, for which root-MUSIC requires some preprocessing [14] (due to loss of Vandermonde structure), and so does ESPRIT [15] (due to loss of shift-invariance). The method, as presented, works best for large ULAs, but can be extended to sparse arrays with relatively few sensor elements, as we shall see in Section III.

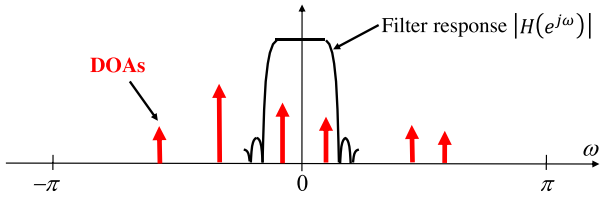

Fig. 2. Typical magnitude response $|H(e^{j\omega})|$, and example of DOA locations (red arrows). Two of the six DOAs are in the passband.

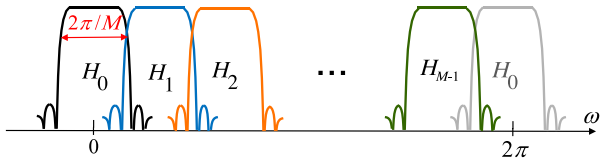

Fig. 3. Typical beamspace filter bank (magnitude responses).

B. Decimating the Filter Output

In classical beamspace methods the complexity advantage is obtained because $B \ll N$. However, for CBS described in the previous section, $N-L+1 \approx N$ since $L \ll N$ in practice. To achieve the complexity reduction of beamspace methods, we simply *decimate* $y(n)$ with a uniform downsampler. Since the passband of $H(z)$ has width $\approx 2\pi/M$ (Fig. 3) we can decimate $y(n)$ by the integer M. For larger arrays, L can be large, and the filters can be designed with sharp cutoff and good stopband attenuation to minimize aliasing due to decimation [32]. Let $v(n) = y(n+L-1)$ so that $\mathbf{y} = [v(0)\ v(1)\ \cdots\ v(N-L)]^T$. Define the decimated version $v_0(n) = v(Mn)$. The vector $\mathbf{y}$ is then replaced by the decimated vector $\bar{\mathbf{v}}_0 = [v(0)\ v(M) \cdots v(J_0 M)]^T$, where $J_0 = \lceil (N-L+1)/M \rceil$. We can estimate the $J_0 \times J_0$ covariance of $\bar{\mathbf{v}}_0$ from snapshots and estimate the D_0 DOAs in the passband, if $D_0 < J_0$. The complexity of eigenspace computation is now

$$O(J_0^3) \ll O(N^3). \tag{8}$$

One might think that decimation leads to "waste" of hard-earned data, but we can make good use of essentially *all* data while estimating a $J \times J$ covariance, where $J = \lfloor (N-L+1)/M \rfloor$. Consider shifted versions $v(n+l)$ for $0 \le l \le M-1$ and define their decimated versions $v_l(n) = v(Mn+l)$. These are the *polyphase components* of $v(n)$ [32]. Let $\mathbf{v}_l = [v_l(0)\ v_l(1)\ \cdots v_l(J-1)]^T$, that is,

$$\mathbf{v}_l = [v(l)\ v(l+M)\ \cdots\ v(l+(J-1)M)\ ]^T. \tag{9}$$

We will estimate $J \times J$ covariances of $\mathbf{v}_l$ and average over all l to obtain a "coherent" estimate of the $J \times J$ covariance of decimated CBS data. Note that we took the floor function of J to accommodate the shorter polyphase components.

C. Decimated Covariance and DOA Estimation

In the following, we develop the decimated covariance matrix. Let $\mathbf{D}_l = [\boldsymbol{\delta}_l\ \boldsymbol{\delta}_{l+M}\ \cdots\ \boldsymbol{\delta}_{l+(J-1)M}]^T$ be a decimation matrix, where $\boldsymbol{\delta}_l$ is the lth standard basis vector for the $(N-L+1)$-dimensional space. Then we can write $\mathbf{v}_l = \mathbf{D}_l \mathbf{y}$. From (6) we have $\mathbf{v}_l = \mathbf{D}_l \mathbf{y} = \mathbf{D}_l \mathbf{A}_L \mathbf{d} + \mathbf{D}_l \mathbf{H} \mathbf{e}$. It can be verified that this simplifies to

$$\mathbf{v}_l = \mathbf{A}_{\rm dec} \mathbf{d}_l + \mathbf{D}_l \mathbf{H} \mathbf{e}, \tag{10}$$

where

$$\mathbf{A}_{\rm dec} = [\mathbf{a}_J(M\omega_1)\ \ \mathbf{a}_J(M\omega_2)\ \cdots\ \mathbf{a}_J(M\omega_D)] \tag{11}$$

with

$$\mathbf{d}_l = \left[c_1 e^{j(L-1+l)\omega_1} H(e^{j\omega_1})\ \cdots\ c_D e^{j(L-1+l)\omega_D} H(e^{j\omega_D}) \right]^T.$$

Thus with $\mathbf{R}_{d_l} = \mathrm{E}[\mathbf{d}_l \mathbf{d}_l^H]$, the covariance of $\mathbf{v}_l$ is

$$\mathbf{R}_{v_l} = \mathrm{E}[\mathbf{v}_l \mathbf{v}_l^H] = \mathbf{A}_{\rm dec} \mathbf{R}_{d_l} \mathbf{A}_{\rm dec}^H + \sigma_e^2 \mathbf{D}_l \mathbf{H} \mathbf{H}^H \mathbf{D}_l^H. \tag{12}$$

It can be verified that the "decimated" matrix

$$\mathbf{G}_{\rm dec} \ \triangleq\ \mathbf{D}_l \mathbf{H} \mathbf{H}^H \mathbf{D}_l \tag{13}$$

is *independent* of l (see Section II-D for details), so

$$\mathbf{R}_{v_l} = \mathbf{A}_{\rm dec} \mathbf{R}_{d_l} \mathbf{A}_{\rm dec}^H + \sigma_e^2 \mathbf{G}_{\rm dec}. \tag{14}$$

The dependency of the first term of (14) on l can be averaged out:

$$\mathbf{R}_{\rm ave} = \frac{1}{M} \sum_{l=0}^{M-1} \mathbf{R}_{v_l} = \mathbf{A}_{\rm dec} \breve{\mathbf{R}}_d \mathbf{A}_{\rm dec}^H + \sigma_e^2 \mathbf{G}_{\rm dec}, \tag{15}$$

where $\breve{\mathbf{R}}_d$ is $\mathbf{R}_{d_l}$ averaged over l. In practice, we estimate $\mathbf{R}_{v_l}$ from snapshots for each l, and then estimate $\mathbf{R}_{\rm ave}$. This is the estimated $J \times J$ covariance to be used for estimating DOAs in the filter passband. Since $\mathbf{v}_l$ for all l are used, *all* the $N-L+1$ components of the CBS signal $\mathbf{y}$ are exploited (if $N-L+1$ is a multiple of M), and no data is wasted. In (15), the Vandermonde structure is preserved, so we can directly use root-MUSIC. ESPRIT is also applicable as shift invariance is retained.

Note that since the columns of $\mathbf{A}_{\rm dec}$ are $\mathbf{a}_J(M\omega_i)$ rather than $\mathbf{a}_J(\omega_i)$, we can only estimate $M\omega_i$ mod 2π, or equivalently

$$\omega_i + 2\pi s_i/M, \tag{16}$$

where the integers s_i are unknown, creating *ambiguity*. But since ω_i are known to be in the passband of $H(e^{j\omega})$ which has width $2\pi/M$, the ambiguities s_i can be resolved because for each DOA, there is only one integer s_i such that $\omega_i + 2\pi s_i/M$ is within the passband. We will show by simulation the effectiveness of this decimation method, as it achieves almost the same performance as that obtained when we do eigenspace computation directly on $\mathbf{y}$, which is of much higher complexity $O(N^3)$.

Remark: One merit of (15) is that the decimated signals are combined "*coherently*." Note that the ith diagonal element of $\breve{\mathbf{R}}_d$ is

$$(\breve{\mathbf{R}}_d)_{ii} = \frac{1}{M} \sum_{l=0}^{M-1} \mathrm{E}[|c_i e^{j(L-1+l)\omega_i} H(e^{j\omega_i})|^2] \tag{17}$$

$$= \frac{1}{M} \sum_{l=0}^{M-1} p_i |H(e^{j\omega_i})|^2 = p_i |H(e^{j\omega_i})|^2, \tag{18}$$

where $p_i = \mathrm{E}[|c_i|^2]$ is the power of the ith source. This explains the "coherent" property of the method as the signal powers $(\breve{\mathbf{R}}_{d_l})_{ii} = p_i |H(e^{j\omega_i})|^2 \ge 0, \forall\ l$ are combined coherently. Actually, when the sources are uncorrelated, $\breve{\mathbf{R}}_{d_l}$ is the same diagonal matrix for all l so that $\breve{\mathbf{R}}_d = \breve{\mathbf{R}}_{d_l}$ for all l, and $\mathbf{R}_{\rm ave}$ in (15) is exactly equal to $\mathbf{R}_{v_l}$ in (14) for all l. Ideally, if we have the exact autocorrelation matrices $\mathbf{R}_{v_l}$, then there is no need to do this average to obtain the same matrix. However, in practice, we only have estimates of $\mathbf{R}_{v_l}$ from snapshots, so this average is helpful to performance. We will show by simulation that this coherent method outperforms the method using only one polyphase component $\mathbf{v}_0$. We will also see that it is also better than the *noncoherent* method, which just computes the average of DOA estimates obtained separately from eigenspace method using each $\mathbf{v}_l$.

D. Spectral Factors of Nyquist Filters to Whiten Noise

The undecimated output of convolution (6) has covariance $\mathbf{R}_{\mathbf{yy}} = \mathbf{A}_L \mathbf{R}_d \mathbf{A}_L^H + \sigma_e^2 \mathbf{G}$, where $\mathbf{R}_d = \mathrm{E}[\mathbf{d}\mathbf{d}^H]$ and $\mathbf{G} = \mathbf{H}\mathbf{H}^H$ is Hermitian and Toeplitz with first row $[g(0)\ g^*(1)\ g^*(2)\ \cdots\ g^*(N-L)]$, where

$$g(k) = \sum_n h(n) h^*(n-k) \tag{19}$$

is the deterministic autocorrelation of $h(n)$. The noise term $\sigma_e^2 \mathbf{G}$ cannot be a diagonal matrix unless the filter has the trivial form $H(z) = cz^{-n_0}$ [32]. But the decimated output (10) has covariance (14) for all l. It can be verified that $\mathbf{G}_{\rm dec} = \mathbf{D}_l \mathbf{H} \mathbf{H}^H \mathbf{D}_l$ is

TABLE I
COMPARISON OF COMPUTATIONAL COMPLEXITY

Algorithm	Complexity	Typical numbers
Element-space MUSIC [9]	$O(N^3 + GN^2)$	3×10^6
Element-space root-MUSIC [10]	$O(N^3)$	10^6
Element-space ESPRIT [11]	$O(N^3)$	10^6
Classical beamspace MUSIC [12]	$O(B^3 + GB^2)$	1.41×10^5
Classical beamspace root-MUSIC [14]	$O(B^3)$	1.56×10^4
Classical beamspace ESPRIT [15]	$O(B^3)$	1.56×10^4
CBS MUSIC [this paper]	$O((N/M)^3 + G(N/M)^2)$	1.41×10^5
CBS root-MUSIC [this paper]	$O((N/M)^3)$	1.56×10^4
CBS ESPRIT [this paper]	$O((N/M)^3)$	1.56×10^4

$J \times J$ Hermitian and Toeplitz with first row

$$[g(0)\ g^*(M)\ g^*(2M)\ \cdots\ g^*((J-1)M)], \tag{20}$$

which is *independent* of l. Thus, whereas $\mathbf{G}$ is the autocorrelation matrix of $h(n)$, the matrix $\mathbf{G}_{\rm dec}$ is constructed from the decimated autocorrelation $g(Mk)$, and does not depend on l. So the corresponding noise term can be whitened by making $\mathbf{G}_{\rm dec} = \mathbf{I}$, or equivalently

$$g(Mk) = \delta(k), \tag{21}$$

where $g(k)$ is as in (19). Eq. (21) is called the *Nyquist*(M) property of $g(k)$. Since $|H(e^{j\omega})|^2$ is the Fourier transform of $g(k)$, we say that $H(z)$ is a *spectral factor* of the Nyquist(M) filter $|H(e^{j\omega})|^2$. In short, by designing the FIR filter $H(z)$ to be a spectral factor of an FIR Nyquist(M) filter $G(z)$ with $G(e^{j\omega}) \geq 0$, we can ensure that the noise terms in the decimated versions $v(Mn + l)$ are white for all l. So $\mathbf{R}_{\rm ave}$ becomes $\mathbf{R}_{\rm ave} = \mathbf{A}_{\rm dec}\breve{\mathbf{R}}_d\mathbf{A}_{\rm dec}^H + \sigma_e^2\mathbf{I}$ where $\mathbf{A}_{\rm dec}$ is as in (11). This makes it easy to find the noise eigenspace by computing eigenvectors of $\mathbf{R}_{\rm ave}$, which is what we do in simulations. Spectral factors of Nyquist filters arise in digital communications [33] and in filter bank theory [32]. There are many ways to design such filters [34]–[37]. In fact, any filter $H_k(e^{j\omega})$ in an *orthonormal* (equivalently paraunitary) filter bank is automatically a spectral factor of a Nyquist filter [32]. Many examples of good FIR designs with this property can be found in the literature [32], [35], [38]–[41]. In fact, if $H(e^{j\omega})$ is a "good" filter with total passband width $\approx 2\pi/M$ and ripples properly constrained, this Nyquist property (21) is approximately satisfied, that is,

$$\sum_{n\neq 0} |g(Mn)| \ll g(0) \quad \text{(nearly-Nyquist property)}. \tag{22}$$

For simplicity, this is what we use in simulations.

In classical beamspace transformation $\mathbf{y} = \mathbf{T}\mathbf{x}$, the orthogonality condition $\mathbf{T}\mathbf{T}^H = \mathbf{I}$ is normally imposed [42]. The Nyquist condition (21) is analogous to this because we are imposing $\mathbf{G}_{\rm dec} = \mathbf{T}\mathbf{T}^H = \mathbf{I}$, where $\mathbf{T} = \mathbf{D}_l\mathbf{H}$.

E. Computational Complexity

The computational complexity of CBS is compared to various methods in the literature in Table I. For element-space root-MUSIC and ESPRIT, the complexity is dominated by the eigenvalue decomposition of the $N \times N$ covariance of the array output $\mathbf{x}$ defined in (1). The complexity is $O(N^3)$. For element-space MUSIC, an additional $O(GN^2)$ is required to compute the MUSIC spectrum $P(\omega) = (\mathbf{a}_N^H(\omega)\mathbf{E}_{\rm n}\mathbf{E}_{\rm n}^H\mathbf{a}_N(\omega))^{-1}$, where $\mathbf{E}_{\rm n}$ is the noise subspace, and G is the number of grid points used for grid search of ω. For classical beamspace, the complexity is dominated by the eigenvalue decomposition of the $B \times B$ covariance of $\mathbf{y} = \mathbf{T}\mathbf{x}$, where $\mathbf{T}$ is a $B \times N$ beamspace transformation matrix. The complexity is $O(B^3)$. Similarly, classical beamspace MUSIC requires an additional $O(GB^2)$ to compute the MUSIC spectrum. For CBS, the complexity is dominated by the eigenvalue decomposition of the covariance (15) for the decimated signals. Assuming the filter length $L \ll N$ so that $(N - L + 1)/M \approx N/M$, the complexity is $O((N/M)^3)$, where M is the decimation ratio. Similarly, CBS MUSIC requires an additional $O(G(N/M)^2)$ to compute the MUSIC spectrum. In Table I, we give an example of typical numbers by setting $N = 100, G = 200, M = 4$, and $B = N/M = 25$. Note that CBS and classical beamspace have the same complexity, which is much smaller than that of element-space. A direct comparison of running time for each algorithm is also presented in Table II.

TABLE II
RUNNING TIME PER MONTE CARLO RUN FOR FIG. 5(C) WHEN $M = 4$ FOR BEAMSPACE METHODS

Algorithm	Running time (sec.)
Classical beamspace	0.00385
MALRD-RLS	0.272
CBS	0.00835
Element-space	0.0840
Element-space with spatial smoothing	0.0945

For all expressions listed in Table I, we include complexity only for computations after the covariance matrices have been estimated using snapshots. For ALRD-RLS and MALRD-RLS [27], the snapshots are used in the RLS algorithm, but no covariance is estimated explicitly. Hence, we do not include ALRD-RLS and MALRD-RLS in Table I, but we list their total complexity here: $O(GK(\bar{B}I^2 + \bar{B}^2))$ for ALRD-RLS and $O(GK(I^2 + \bar{B}^2))$ for MALRD-RLS, where I is the length of the basis vectors contained in the $\bar{B} \times N$ beamspace transformation matrix $\mathbf{T}$, K is the number of snapshots, and G is the number of grid points used for grid search of ω. Note that we use the notation $\bar{B}$ as it may be different from B for other algorithms. To compare ALRD-RLS and MALRD-RLS with other algorithms, we need to include complexity for estimating the covariance also. For instance, for classical beamspace root-MUSIC, the complexity of $\mathbf{y} = \mathbf{T}\mathbf{x}$ for K snapshots, where $\mathbf{T}$ is a $B \times N$ matrix, is either $O(KNB)$, or $O(KN\log_2 N)$ if rows of $\mathbf{T}$

are chosen to be columns of the DFT matrix so that the FFT algorithm can be used. Estimating the $B \times B$ covariance of $\mathbf{y}$ using K snapshots then requires $O(KB^2)$ computation. Thus, the total complexity is $O(B^3 + KB^2 + KN\min(B, \log_2 N))$. But from this expression, it is more tricky to obtain typical numbers as in Table I because the constant factors of each term in the big-O notation are hidden.

F. Error Analysis

Now we analyze the performance of CBS with decimation. This is only an approximate analysis of the mean square error (MSE) of the DOA estimates, but it provides insights. For simplicity, we consider the MUSIC algorithm here, although the simulations presented later use root-MUSIC or ESPRIT. Let $\hat{\omega}_i$ be the estimate of the ith DOA ω_i, $1 \le i \le D$. When MUSIC is performed on an N-sensor ULA with K snapshots in element-space, the estimate $\hat{\omega}_i$ is asymptotically (for large K and N) unbiased and has variance [18]

$$\mathrm{var}_{\mathrm{elm}}(\hat{\omega}_i) = \frac{6\sigma_e^2}{KN^3}(\mathbf{R}_{\mathbf{cc}}^{-1})_{ii}, \tag{23}$$

where $\mathbf{R}_{\mathbf{cc}} = \mathrm{E}[\mathbf{c}\mathbf{c}^H]$ is the autocorrelation of the source amplitudes. In particular, if the sources are uncorrelated with powers σ_i^2, then we have

$$\mathrm{var}_{\mathrm{elm}}(\hat{\omega}_i) = \frac{6\sigma_e^2}{KN^3\sigma_i^2}. \tag{24}$$

For simplicity, consider CBS with decimation using only one polyphase component, and suppose the decimation ratio M is a divisor of $(N - L + 1)$, so

$$J = (N - L + 1)/M \tag{25}$$

is an integer. Suppose the filter $H(e^{j\omega})$ satisfies the nearly-Nyquist property (22) so that $\mathbf{G}_{dec} \approx \mathbf{I}$. Let $H(e^{j\omega})$ be a good filter with passband $[-\pi/M, \pi/M]$, i.e.,

$$|H(e^{j\omega})|^2 \approx \begin{cases} M, & |\omega| < \pi/M \\ 0, & \text{otherwise} \end{cases} \tag{26}$$

so that it has unit energy. For CBS with decimation, since the columns of $\mathbf{A}_{dec}$ are $\mathbf{a}_J(M\omega_i)$ rather than $\mathbf{a}_J(\omega_i)$, so in view of (14), for an in-band DOA ω_i (DOA in the passband of the filter),

$$\mathrm{var}_{\mathrm{CBS}}(M\hat{\omega}_i) \approx \frac{6\sigma_e^2}{KJ^3|H(e^{j\omega_i})|^2\sigma_i^2}. \tag{27}$$

Using (25), (26), and the fact that $\mathrm{var}(cx) = c^2\mathrm{var}(x)$ for any constant $c > 0$ and random variable x, we therefore obtain

$$\mathrm{var}_{\mathrm{CBS}}(\hat{\omega}_i) \approx \frac{6\sigma_e^2}{K(N - L + 1)^3\sigma_i^2}. \tag{28}$$

Moreover, if the filter length $L \ll N$,

$$\mathrm{var}_{\mathrm{CBS}}(\hat{\omega}_i) \approx \frac{6\sigma_e^2}{KN^3\sigma_i^2} = \mathrm{var}_{elm}(\hat{\omega}_i). \tag{29}$$

Thus, the error variance of CBS is approximately independent of the decimation ratio M and equal to that of element-space. Hence, one may want to choose a large M to lower computational complexity. However, there is some price to be paid for this advantage. Since the number of identifiable sources is limited by $J = (N - L + 1)/M$, large M means fewer sources can be identified in the passband. Secondly, since a large M implies that the filter has narrower pass and transition bands, the stop band attenuation degrades for large M (for fixed filter length L).

The above analysis is valid as long as all the in-band sources are uncorrelated. Whether an in-band source is correlated with an out-of-band source (source in the stopband) or not does not matter. This also suggests how *CBS can improve performance over element-space*. For illustration, consider an example where there is one in-band source with power 1 and one out-of-band source with power P_{o}, with correlation coefficient $0 < \rho < 1$. Hence,

$$\mathbf{R}_{\mathbf{cc}} = \begin{bmatrix} 1 & \rho\sqrt{P_{\mathrm{o}}} \\ \rho\sqrt{P_{\mathrm{o}}} & P_{\mathrm{o}} \end{bmatrix}, \tag{30}$$

and

$$\mathbf{R}_{\mathbf{cc}}^{-1} = \frac{1}{(1-\rho^2)P_{\mathrm{o}}} \begin{bmatrix} P_{\mathrm{o}} & -\rho\sqrt{P_{\mathrm{o}}} \\ -\rho\sqrt{P_{\mathrm{o}}} & 1 \end{bmatrix}, \tag{31}$$

so it can be derived from (23) that

$$\mathrm{var}_{\mathrm{elm}}(\hat{\omega}_1) = \frac{6\sigma_e^2}{KN^3(1-\rho^2)}. \tag{32}$$

The error variance for element-space gets larger as ρ gets larger, but is independent of the out-of-band power P_{o}. By contrast, for CBS, as long as the out-of-band source is attenuated enough by the filter so that the in-band source is the only effective source after filtering, then it is as if there is only the first source, or its effective $\mathbf{R}_{\mathbf{cc},\mathrm{CBS}}$ is a 1×1 matrix $\mathbf{R}_{\mathbf{cc},\mathrm{CBS}} = 1$. Hence, setting $\sigma_1^2 = 1$ in (29), we obtain

$$\mathrm{var}_{\mathrm{CBS}}(\hat{\omega}_1) \approx \frac{6\sigma_e^2}{KN^3} < \mathrm{var}_{elm}(\hat{\omega}_1). \tag{33}$$

It is important to note that this does not contradict the analysis for beamspace MUSIC in [42], [43] because therein the signal subspace dimension in the beamspace is assumed to be the same as that in the element-space, but for CBS, signal subspace dimension after filtering can be smaller. That is, in [42], [43], all sources, including those in the stopband if any, still have to be estimated in the beamspace, while in our case we only have to estimate in-band ones. Besides, (33) does not contradict the fact that the beamspace Cramer-Rao bound (CRB) cannot be smaller than the element-space CRB [43] because the gap between the error variance of a practical algorithm and the CRB can differ in different situations. The foregoing example shows that CBS can improve MUSIC MSE performance in some cases when there are correlated sources.

Remark: A more rigorous analysis will have error variance expressions involving $H(e^{j\omega})$. The filtered out-of-band sources contribute to error terms that perturb the eigenvectors of the covariance matrix. Such an error term is not white and may be correlated with in-band sources. This makes a rigorous analysis complicated, and we leave it for future work. From a practical point of view, observe that if $H(e^{j\omega})$ is designed to have good stopband attenuation, then the error term due to filtered out-of-band sources is much smaller than the white noise term, and the analyses in this subsection can be good approximations.

G. Simulations

In all simulation examples in this paper, we assume the number of DOAs is unknown. For CBS, the number of in-band DOAs D_0 has to be estimated. For element-space, the number of all DOAs D has to be estimated. For CBS method to estimate D_0, we plot the distribution of eigenvalues of the covariance $\mathbf{R}_{\mathrm{ave}}$ in descending order in log scale, and the most convex point (maximum of the second difference) of the curve is regarded as the first noise subspace eigenvalue. Then, the

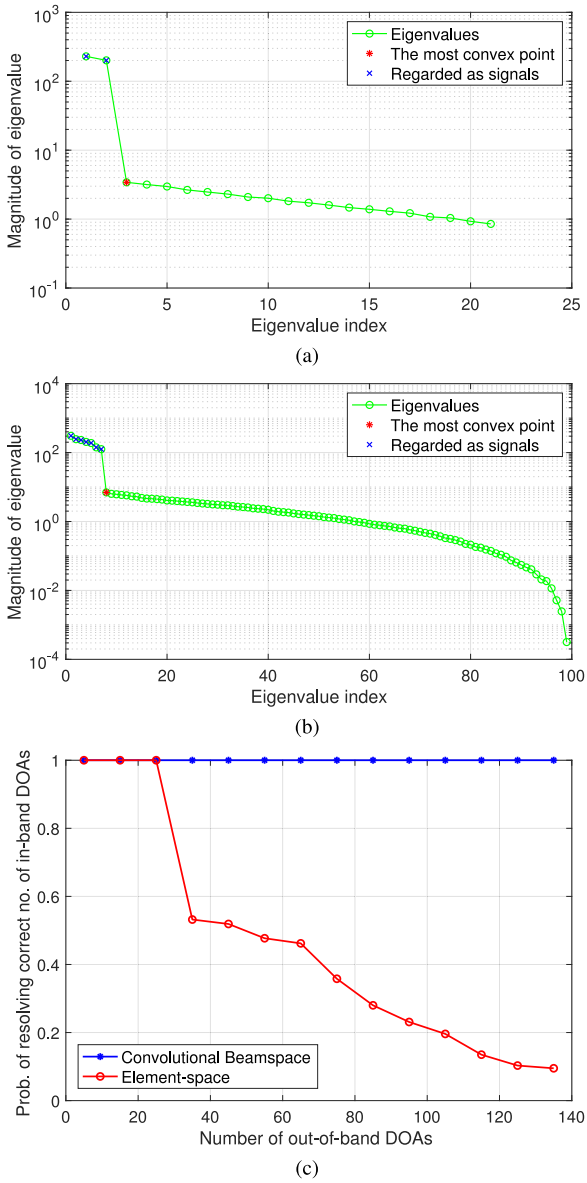

Fig. 4. Performance of CBS and element-space when there are many out-of-band DOAs. (a) Typical eigenvalue distribution for CBS. (b) Typical eigenvalue distribution for element-space. (c) Probability of resolution.

number of eigenvalues larger than this is the estimated D_0. For element-space to estimate D, the same method is used, with $\mathbf{R}_{\text{ave}}$ replaced by the covariance of the original array output $\mathbf{x}$. See Fig. 4(a)–(b) for a numerical demonstration (details of this plot will be described below). To compare with CBS using a filter $H(z)$, for element-space, we just consider DOA estimates in the passband of $H(z)$ and ignore those in the stopband. The number of in-band DOAs obtained in this way is also viewed as the estimate of D_0 for element-space.

Whenever we mention root mean square errors (RMSE) in detected in-band source angles, we refer to averaging square errors measured in ω over all in-band DOAs and over those Monte Carlo runs that obtain the correct number of in-band DOAs. Similarly, since the stochastic Cramer-Rao bounds (CRBs) [44] depend on DOAs, we have averaged over in-band DOAs in the plots. Noise variance $\sigma_e^2 = 1$ is used. If not specified particularly, the following settings are used for each example. First, all sources are uncorrelated with equal powers $p_k = 1$. Second, the coherent method (15) is used for CBS with decimation. Third, $H(z)$ is designed to be lowpass using the Parks-McClellan algorithm [28], with passband edge $\pi/2M$ and stopband edge $3\pi/2M$. Here their average π/M is viewed as the filter *cutoff*, and M is the decimation ratio. These Parks-McClellan filters satisfy (22).

Probability of resolution. We first consider a scenario where there are many out-of-band DOAs. In this case, CBS is especially advantageous over element-space in terms of probability of resolution. Consider a ULA with $N = 99$ sensors. The filter length is $L = 16$, and the decimation ratio is $M = 4$. There are two in-band DOAs, which are at angles $\theta = -5^\circ, 5^\circ$. We vary the number of out-of-band DOAs $\bar{D}$, while they are uniformly placed in the range $\omega \in [0.5\pi, 0.98\pi]$, i.e., $\omega = 0.5\pi, 0.5\pi + \delta, 0.5\pi + 2\delta, \ldots, 0.98\pi$ with $\delta = 0.48\pi/(\bar{D} - 1)$. (Recall $\omega = \pi \sin\theta$.) Fig. 4(c) shows the probability of resolving the correct number of in-band DOAs using the method of finding the most convex point of eigenvalue distribution. Typical eigenvalue distributions for a Monte Carlo run are shown in Fig. 4(a)–(b) when there are 5 out-of-band DOAs. Note that 2 and 7 eigenvalues are regarded as signals for CBS and element-space, respectively, corresponding to the number of in-band DOAs and all DOAs. Covariance estimates are obtained by using 100 snapshots, and we average 1000 Monte Carlo runs to get the plot. As expected, for CBS, the number of out-of-band DOAs does not affect the probability of resolution, which is always 1 in this example, because they are attenuated by the filter. Even when the number of out-of-band DOAs is greater than the number of sensors $N = 99$, CBS can still recover the in-band DOAs with probability one. But for element-space, the probability of resolution decreases significantly as the number of out-of-band DOAs increases.

Estimation errors. We now compare the estimation errors of classical beamspace [14], MALRD-RLS [27], CBS, and element-space. Consider a ULA with $N = 96$ sensors receiving 6 sources at angles $-3^\circ, 1.5^\circ, 3^\circ, 40^\circ$, 60°, and 80°. The filter length is $L = 25$, and the decimation ratio M is varied. Filter responses for some M are shown in Fig. 5(a). For all filters used, there are three sources in the passband ($-3^\circ, 1.5^\circ$ and 3°) and three in the stopband ($40^\circ, 60^\circ$, and 80°). All sources are first assumed uncorrelated. For MALRD-RLS, the parameters (as mentioned in the last paragraph of Section II-E) are reasonably chosen as per [27]. Specifically, we set $I = 12$, $\bar{B} = N/I$, and the forgetting factor $\alpha = 0.998$ as in [27]. The number of grid points for grid search of ω is chosen as $G = 1000$ to keep a balance between performance and complexity. For MALRD-RLS, the number of DOAs and their locations are estimated together based on the *output power spectrum* $P(\omega)$ [27]. We declare that there is a source at $\bar{\omega}$ if $P(\bar{\omega})$ is a local maximum with prominence greater than 0.4 (with the spectrum normalized to have a maximum value 1), where prominence is defined as in `findpeaks` of MATLAB. In all cases experimented except MALRD-RLS, the probability of resolving the correct number of in-band DOAs is always 1, so it is not plotted. MALRD-RLS failed to resolve only once in 500 trials, so the probability of success is nearly unity as well. We turn to study the RMSE in detected in-band source angles using root-MUSIC, for various values of $1/M$ (filter cutoff normalized by π), as

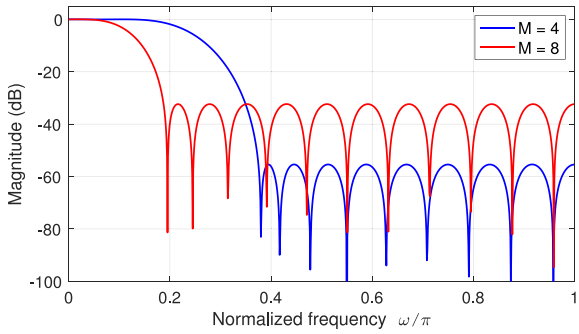

(a)

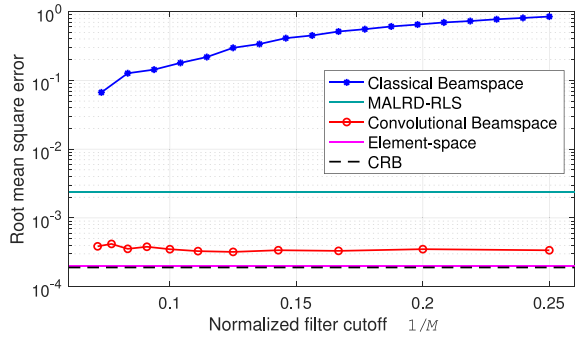

(b)

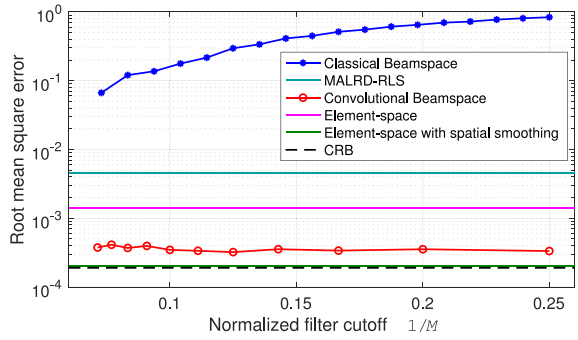

(c)

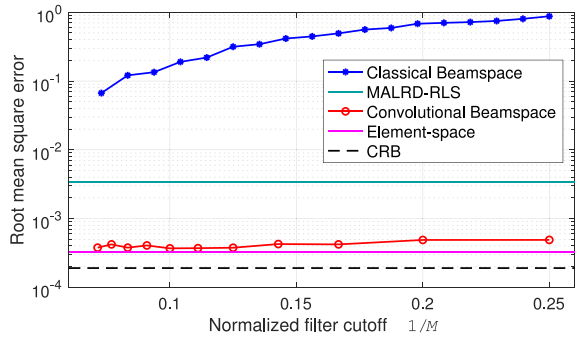

(d)

Fig. 5. RMSE of classical beamspace, MALRD-RLS, CBS, and element-space. (a) Responses of typical filters used. (b) RMSE for uncorrelated sources. (c) RMSE for in-band sources correlated with out-of-band sources. (d) RMSE for correlated in-band sources.

shown in Fig. 5(b). Covariance estimates are obtained by using 200 snapshots, and 500 Monte Carlo runs are used. Note that, for MALRD-RLS and element-space, the notion of filter cutoff is not relevant, so their plots are constant. CBS outperforms classical beamspace [14], the poor performance of the latter being consistent with numerical sensitivity issues mentioned in [14] as the number of "beams" B (i.e., passband width in our notion) increases. CBS also outperforms MALRD-RLS. Note that element-space performs slightly better, and that the RMSE is almost independent of M for CBS, consistent with (24) and (28). Fig. 5(c) shows the performance when there are in-band sources *correlated* with out-of-band sources: sources n and $n+3$ have a correlation coefficient $\rho = 0.85$ for $n = 1, 2, 3$. In this case, CBS outperforms element-space significantly (without spatial smoothing), consistent with (33). Again, this does not contradict [42], [43] as we explained for (33). Note that we also show the RMSE of element-space using spatial smoothing [45]. We divide the array into 6 overlapping subarrays of size 91: $\{1, \ldots, 91\}$, $\{2, \ldots, 92\}, \ldots, \{6, \ldots, 96\}$, and then do spatial smoothing. Although spatial smoothing can achieve performance improvement for correlated sources, only CBS can achieve both performance improvement and complexity reduction (see Table II). This is because spatial smoothing does not do dimensionality reduction (unlike CBS). Stochastic (element-space) CRBs [44] are also shown in Fig. 5(b)–(c). While both CBS and element-space come close to the CRB for uncorrelated sources, only CBS comes close to the CRB for correlated sources. CBS fills in the gap between element-space (without spatial smoothing) and CRB for correlated sources. The running time per Monte Carlo run for each algorithm in Fig. 5(c) is shown in Table II. The computational complexity of CBS is comparable to that of classical beamspace and more than 10 times lower than that of element-space (with or without spatial smoothing). Running time of MALRD-RLS depends on the number of grid points G for grid search of ω. As mentioned before, we have chosen $G = 1000$, and the complexity of MALRD-RLS is the highest. This choice of G was necessary to obtain the reasonable performances shown in Fig. 5. On the other hand, performances cannot be significantly improved by a larger G. For instance, the RMSE for Fig. 5(b) would change from 0.0023 only to 0.0021 if G is changed from 1000 to 10000, but the complexity gets much higher. Finally, we consider the case when there are in-band correlated sources in Fig. 5(d). Here, sources 1 and 2 are correlated with $\rho = 0.85$ and all others are uncorrelated. CBS again outperforms classical beamspace and MALRD-RLS. Although CBS does not outperform element-space as in Fig. 5(c), it is only slightly worse than element-space, and both of them are reasonably close to the CRB.

Truncation versus decimation. Next, we show that decimating the filter output is indeed an effective method. To this end, we compare CBS with decimation (15), CBS with *truncation*, and element-space. "CBS with truncation" means we keep only the first $N_{bs} \leq N - L + 1$ samples of the filter output, $v(0), v(1), \ldots, v(N_{bs} - 1)$. Consider a ULA with $N = 99$ sensors receiving 2 in-band sources at angles $-5^\circ, 5^\circ$, and 1 out-of-band source at angle 40°. The filter length is $L = 16$, and the decimation ratio is $M = 4$. Fig. 6 shows the RMSE in detected in-band source angles using root-MUSIC. Covariance estimates are obtained by using 100 snapshots, and 500 Monte Carlo runs are used. As expected, for the truncated CBS, RMSE decreases as N_{bs} increases. Remarkably, the RMSE at $N_{bs} = 84$, corresponding to keeping all the steady-state samples of the filter output, is about the same as the RMSE of CBS with decimation by $M = 4$. Moreover, CBS with decimation gives a RMSE almost the same as element-space, as suggested by (29). So in

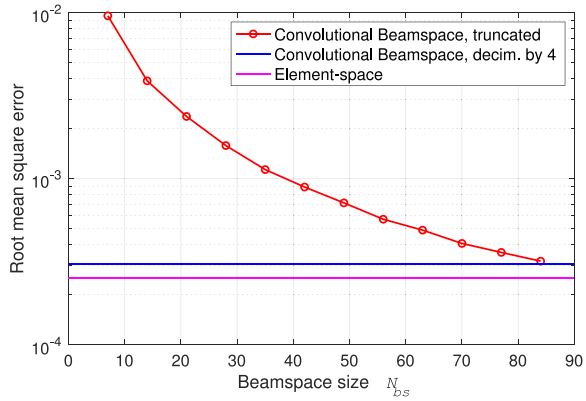

Fig. 6. RMSE of truncated CBS, decimated CBS, and element-space.

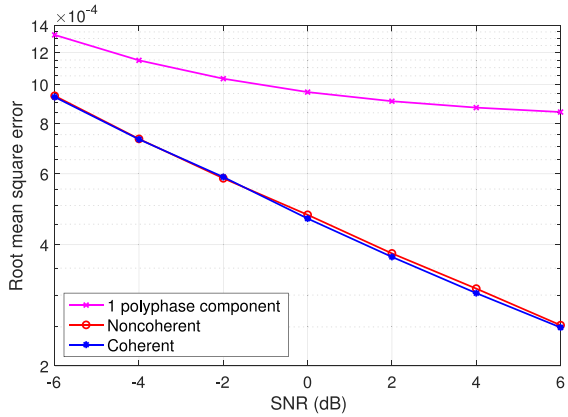

Fig. 7. RMSE of CBS using all polyphase components coherently and noncoherently, versus using only one polyphase component.

the decimation method, the only loss is due to discarding the transient part of the filter output, which is insignificant if $L \ll N$. Hence, decimation reduces the complexity of eigenspace computation by a factor of $O(M^3)$ without compromising the RMSE performance!

Coherent versus noncoherent. Finally we compare the coherent method (15) with the noncoherent method, and with the method which uses only one polyphase component. Consider a ULA with $N = 99$ sensors. The filter length is $L = 16$, and the decimation ratio is $M = 12$. Two in-band sources are at angles $\theta = -0.5^\circ, 0.5^\circ$, and 30 out-of-band sources are uniformly placed in the range $\omega \in [0.5\pi, 0.98\pi]$. Fig. 7 shows the RMSE in detected in-band source angles using root-MUSIC. Covariance estimates are obtained by using 100 snapshots, and 5000 Monte Carlo runs are used. Indeed, the RMSE of the coherent method is slightly smaller than that of the noncoherent method, and is much smaller than that of using only one polyphase component.

III. Convolutional Beamspace for Sparse Arrays

In this section, we show that CBS can be also applied to sparse arrays. In Section III-A, the idea of difference coarrays for sparse arrays is reviewed. In Section III-B, we show how to do CBS in the coarray domain, as depicted in (40) or (41). In Section III-C, we show that we can again use uniform decimation to reduce computational complexity, and the decimated output (44) still has the Vandermonde structure of the ULA output. Hence, root-MUSIC and ESPRIT can be directly applied to the filtered and decimated coarray output without further adjustment. A brief discussion of computational complexity is given in Section III-D. Finally, simulations are presented in Section III-E.

Consider linear arrays for which the sensor locations are at $n\lambda/2$ where $n \in \mathcal{N} = \{n_0, n_1, \ldots, n_{N-1}\}$. The integer set $\mathcal{N}$ defines the array. For a ULA, we have $\mathcal{N} = \{0, 1, 2, \cdots, N-1\}$. More generally $\mathcal{N}$ can be a sparse array like the nested array [20], coprime array [21], or minimum redundancy array (MRA) [19]. One advantage of sparse arrays over ULAs is that it is possible to estimate $O(N^2)$ DOAs using an N-sensor sparse array [20].

Let $x(n_i), 0 \le i \le N-1$ be the array output. One can still use a filter $h(i)$ to perform a "convolution" as before, that is, $y(m) = \sum_i x(n_i)h(m-i)$. But this is not useful because the array output in response to a single DOA has the form $x(n_i) = ce^{j\omega n_i} \neq e^{j\omega i}$ (except for a ULA). So the vector $\mathbf{x} = [x(n_0) \cdots x(n_{N-1})]$ is not Vandermonde, and Eqs. (4) and (5) are not true. So a filtering effect like $H(e^{j\omega_k})\mathbf{a}_{N-L+1}(\omega_k)$ cannot be achieved in this way. But we will have better luck working in the difference coarray domain. This is similar in principle to the idea in [46] for classical beamspace.

A. Difference Coarrays

With the array output

$$x(n_i) = \sum_{k=1}^{D} c_k e^{j\omega_k n_i} + e(n_i), \quad n_i \in \mathcal{N}, \tag{34}$$

the cross-correlation between outputs of sensors n_i and n_m is

$$\mathrm{E}[x(n_i)x^*(n_m)] = \sum_{k=1}^{D}\sum_{l=1}^{D} \mathrm{E}[c_k c_l^*] e^{j(\omega_k n_i - \omega_l n_m)} + \sigma_e^2 \delta(n_i - n_m) \tag{35}$$

under standard statistical assumptions mentioned in Section II. For zero-mean uncorrelated sources, $\mathrm{E}[c_k c_l^*] = p_k \delta(k-l)$, where $p_k = \mathrm{E}[|c_k|^2]$ is the power of the kth source. So

$$\begin{aligned} R(n_i - n_m) &\triangleq \mathrm{E}[x(n_i)x^*(n_m)] \\ &= \sum_{k=1}^{D} p_k e^{j\omega_k(n_i - n_m)} + \sigma_e^2 \delta(n_i - n_m), \end{aligned}$$

which depends only on the difference $n_i - n_m$ between sensor locations, hence the notation $R(n_i - n_m)$. The *difference coarray* $\mathcal{C}$ of the array $\mathcal{N} = \{n_i\}$ is the set of all possible differences $n_i - n_m$ between sensor locations. By estimating $\mathrm{E}[x(n_i)x^*(n_m)]$ using snapshot averages, we can estimate

$$R(l) = \sum_{k=1}^{D} p_k e^{j\omega_k l} + \sigma_e^2 \delta(l) \tag{36}$$

for all $l \in \mathcal{C}$. The difference coarray is symmetric in the sense that if $l \in \mathcal{C}$, then $-l \in \mathcal{C}$. Let the largest element in $\mathcal{C}$ be Z, and let U be the largest integer such that the uniform region $-(U-1) \le l \le U-1$ is in $\mathcal{C}$. Then $-(U-1) \le l \le U-1$ is called the *central ULA segment* of the difference coarray. If $U < Z$, the region $U \le l \le Z-1$ contains some integers which do not belong in $\mathcal{C}$, called *holes* in the coarray, and in particular U is a hole. Note that for an array with hole-free coarray (like the nested array), the coarray itself is the central ULA segment.

Since (36) can be estimated for all $l \in \mathcal{C}$, we can in particular estimate $R(l)$ over the central ULA segment $-(U-1) \le l \le U-1$, and define a Hermitian Toeplitz matrix

$$\mathbf{R} = \begin{bmatrix} R(0) & R^*(1) & \cdots & R^*(U-1) \\ R(1) & R(0) & \cdots & R^*(U-2) \\ \vdots & \vdots & \ddots & \vdots \\ R(U-1) & R(U-2) & \cdots & R(0) \end{bmatrix}. \tag{37}$$

All elements of the matrix can be estimated by averaging $x(n_i)x^*(n_m)$ over snapshots, and over all n_i, n_m that produce identical difference $l = n_i - n_m$. This estimate of $\mathbf{R}$ was denoted as $\widetilde{\mathbf{R}}$ in [47]. By computing the noise eigenspace of $\widetilde{\mathbf{R}}$ we can estimate the DOAs ω_k using standard methods such as MUSIC. In general, $\widetilde{\mathbf{R}}$ may fail to be positive definite because it is a finite snapshot estimate. But it is shown in [47] that if we order its eigenvalues in terms of their absolute values and define the noise subspace accordingly, this always works.

B. Convolutional Beamspace in the Coarray Domain

Consider an FIR filter $G(z) = H(z)H^*(1/z^*)$ where $H(z) = \sum_{n=0}^{L-1} h(n)z^{-n}$ so that $G(e^{j\omega}) = |H(e^{j\omega})|^2 \ge 0$. We have

$$G(z) = \sum_{k=-L+1}^{L-1} g(k)z^{-k}, \tag{38}$$

where $g(k) = \sum_n h(n)h^*(n-k)$ and $g(k) = g^*(-k)$. Assume $L < U$ and define the finite duration signal

$$R^{(u)}(l) = \begin{cases} R(l), & -(U-1) \le l \le U-1 \\ 0, & \text{otherwise.} \end{cases} \tag{39}$$

where $R(l)$ is as in (36). This is $R(l)$ restricted to the central ULA portion of the coarray, hence the superscript "(u)". Now consider the convolution

$$R_0(n) = \sum_{l=-(U-1)}^{U-1} R^{(u)}(l)g(n-l), \tag{40}$$

which can be nonzero in $-(U+L-2) \le n \le U+L-2$. In the restricted range $\mathcal{S} = \{n | -(U-L) \le n \le U-L\}$, we have

$$\underbrace{\begin{bmatrix} R_0(-(U-L)) \\ R_0(-(U-L-1)) \\ \vdots \\ R_0(U-L) \end{bmatrix}}_{\mathbf{r}_0} = \mathbf{G}_{\text{co}} \underbrace{\begin{bmatrix} R(-(U-1)) \\ R(-(U-2)) \\ \vdots \\ R(U-1) \end{bmatrix}}_{\mathbf{r}}, \tag{41}$$

where $\mathbf{G}_{\text{co}}$ is the banded Toeplitz matrix

$$\begin{bmatrix} g(L-1) & \cdots & g(-(L-1)) & 0 & \cdots & 0 \\ 0 & \ddots & & \ddots & \ddots & \vdots \\ \vdots & \ddots & & & & 0 \\ 0 & \cdots & 0 & g(L-1) & \cdots & g(-(L-1)) \end{bmatrix}$$

of size $(2(U-L)+1) \times (2U-1)$. Thus, all the $2L-1$ filter coefficients $g(k)$ are involved in the computation of $R_0(n)$ in $n \in \mathcal{S}$, so that $\mathbf{r}_0$ in (41) defines the *steady state* portion of the output. We refer to $\mathbf{r}_0$ as the *coarray convolutional beamspace* signal generated from the ULA segment $\mathbf{r}$ of the coarray. In this steady state, we can readily verify that

$$R_0(n) = \sum_{k=1}^{D} p_k G(e^{j\omega_k}) e^{j\omega_k n} + \sigma_e^2 g(n), \quad n \in \mathcal{S}. \tag{42}$$

Since $p_k G(e^{j\omega}) \ge 0$, the quantity $R_0(n)$ in (42) resembles the autocorrelation of a sum of sinusoids buried in noise with autocorrelation $\sigma_e^2 g(n)$, and in particular $R_0(n) = R_0^*(-n)$. The DOA ω_k is filtered by $G(e^{j\omega_k})$, so if $G(e^{j\omega})$ is a good lowpass filter with passband width $\approx 2\pi/M$, then

$$R_0(n) \approx \sum_{k=1}^{D_0} p_k G(e^{j\omega_k}) e^{j\omega_k n} + \sigma_e^2 g(n), \quad n \in \mathcal{S}, \tag{43}$$

where D_0 is the number of sources falling within the passband of the filter $G(e^{j\omega})$.

In summary, the DOAs in a narrow subband can be isolated by this coarray filtering. Restricting the filtering to the ULA portion of the coarray (as in (39)) and considering only the outputs in the steady state $\mathcal{S}$, we ensure the exact relation (42). Since the filter, by design, satisfies $G(e^{j\omega}) \ge 0$, (42) is still a valid autocorrelation truncated to $\mathcal{S}$. Since the steady state domain $\mathcal{S}$ still looks like a ULA (i.e., (42) has the Vandermonde structure with respect to $n \in \mathcal{S}$), we can directly apply root-MUSIC or ESPRIT without any additional steps. As U is typically as large as $O(N^2)$, we can design a sharp-cutoff filter with good stopband attenuation by using a relatively long filter length L.

C. Decimating in the Coarray Domain

Since the filter $G(e^{j\omega})$ has passband width $\approx 2\pi/M$, we can work with the uniformly decimated version

$$R_0(Mn) = \sum_{k=1}^{D} p_k G(e^{j\omega_k}) e^{jM\omega_k n} + \sigma_e^2 g(Mn) \tag{44}$$

with n restricted such that $Mn \in \mathcal{S}$. Decimation achieves the dimensionality reduction needed to reduce the computational complexity in the subbands, such reduction being an integral part of any beamspace processing. If $G(e^{j\omega})$ is *Nyquist*(M), then $g(Mn) = \delta(n)$ and

$$\begin{aligned} R_0(Mn) &= \sum_{k=1}^{D} p_k G(e^{j\omega_k}) e^{jM\omega_k n} + \sigma_e^2 \delta(n) \\ &\approx \sum_{k=1}^{D_0} p_k G(e^{j\omega_k}) e^{jM\omega_k n} + \sigma_e^2 \delta(n). \end{aligned} \tag{45}$$

Since the noise term has $\delta(n)$ and $p_k G(e^{j\omega_k}) \ge 0$, Eq. (45) represents the autocorrelation of a sum of sinusoids buried in *white* noise. We now define a $q \times q$ Hermitian Toeplitz matrix (where q is the largest integer with $(q-1)M \in \mathcal{S}$):

$$\begin{bmatrix} R_0(0) & R_0^*(M) & \cdots & R_0^*((q-1)M) \\ R_0(M) & R_0(0) & \cdots & R_0^*((q-2)M) \\ \vdots & \vdots & \ddots & \vdots \\ R_0((q-1)M) & R_0((q-2)M) & \cdots & R_0(0) \end{bmatrix}.$$

Its eigendecomposition reveals the noise subspace from which the frequencies $M\omega_k \pmod{2\pi}$ can be identified (when $D_0 < q$). From these we can identify ω_k without ambiguity as before, by using the fact that only those ω_k that are in the passband of $G(e^{j\omega})$ contribute significantly to $R_0(n)$. Again, for finite snapshots, we order eigenvalues in terms of their absolute values to define noise subspace [47].

As before, instead of using one filter $G(e^{j\omega}) \ge 0$, we can use a filter bank $G_i(e^{j\omega}), 0 \le i \le M-1$ with filter responses covering the range $0 \le \omega < 2\pi$ as in Fig. 3. We now constrain $G_i(e^{j\omega})$ to be Nyquist(M) with $G_i(e^{j\omega}) \ge 0$. Using these we

TABLE III
RUNNING TIME PER MONTE CARLO RUN FOR COARRAY BASED CBS FOR SPARSE ARRAYS (FIG. 8) WHEN THERE ARE 80 OUT-OF-BAND DOAS

Algorithm	Running time (sec.)
CBS ESPRIT	0.00646
Element-space ESPRIT	0.0447
Classical beamspace root-MUSIC	0.0109
Classical beamspace ESPRIT	0.00796

obtain the *decimated coarray CBS* signals $R_i(Mn), 0 \le i \le M-1$. Analysis of the ith signal $R_i(Mn)$ reveals the D_i DOAs falling into the ith subband. The union of these DOAs gives the set of all D DOAs.

D. Computational Complexity

The computational advantage of CBS for sparse arrays is similar to CBS for ULAs. With $-(U-1) \le l \le U-1$ being the central ULA segment of the difference coarray, the complexity of eigenspace computation for CBS is $O((U/M)^3)$, which is much smaller than $O(U^3)$, the complexity of eigenspace computation for element-space. (Here, we work in the coarray domain for both CBS and element-space. So, in this section element-space means "coarray domain without filtering.") A direct comparison of running time for CBS, element-space, and classical beamspace is also presented in Table III.

E. Simulations

We consider an example where the number of in-band DOAs is greater than the number of sensors, which is a scenario that makes sparse arrays stand out. A two-level nested array [20] with each level having 12 sensors is considered, a total of 24 sensors. CBS ESPRIT is compared with element-space ESPRIT, classical beamspace root-MUSIC [14], and classical beamspace ESPRIT [15]. We follow the procedure in [46] to do classical beamspace in the coarray domain. The covariance in the beamspace is computed by $\mathbf{TRT}^H$, where $\mathbf{T}$ is the beamspace transformation matrix, and $\mathbf{R}$ is defined in (37). For CBS, a Parks-McClellan filter $H(z)$ of length $L = 16$ and with cutoff π/M is used, where $M = 4$ is the decimation ratio. So the filter $G(z)$ in (38) has length 31. There are 25 in-band DOAs, uniformly placed in the range $\omega \in [-0.2\pi, 0.2\pi]$. We vary the number of out-of-band DOAs, while they are uniformly placed in $\omega \in [0.5\pi, 0.98\pi]$. Covariance estimates are obtained by using 1000 snapshots, and 5000 Monte Carlo runs are used. Fig. 8(a) shows the probability of resolving the correct number of in-band DOAs. CBS consistently offers a larger probability of resolution than element-space and classical beamspace root-MUSIC and ESPRIT, as the number of out-of-band DOAs varies. Moreover, as shown in Fig. 8(b), CBS has the smallest average of absolute values of bias in detected in-band source angles. Finally, Fig. 8(c) shows that compared to element-space and classical beamspace ESPRIT, CBS has similar RMSE in detected in-band source angles when there are fewer out-of-band DOAs. But, CBS has significantly smaller RMSE when there are more out-of-band DOAs. Note that classical beamspace root-MUSIC always has zero probability of resolution due to numerical sensitivity issues [14] as we have a large coarray size $U = 156$; so we do not plot its bias and RMSE in Fig. 8(b)–(c). The running time per Monte Carlo run for each algorithm is shown in Table III. The

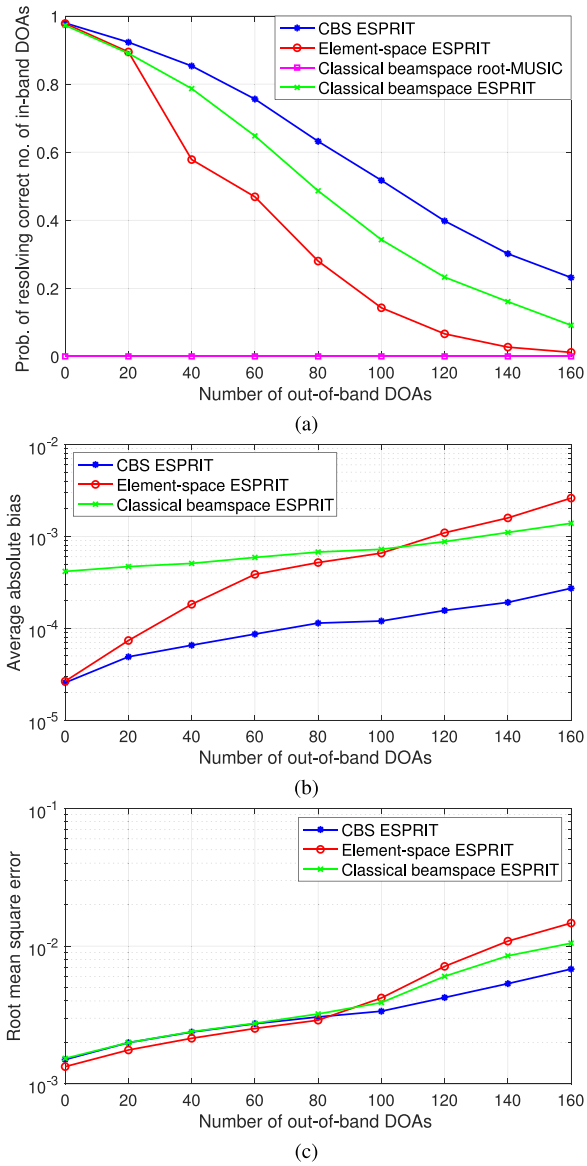

Fig. 8. Performance of CBS in coarray domain, and element-space in coarray domain for sparse arrays using ESPRIT. The classical beamspace method in the coarray domain [46] is also compared using both root-MUSIC and ESPRIT. A nested array [20] with 24 sensors was used. (a) Probability of resolution. (b) Average absolute bias. (c) RMSE.

computational complexity of CBS is a little lower than that of classical beamspace and about 7 times lower than that of element-space. This example shows that for the typical scenario of resolving more sources than sensors using sparse arrays, many benefits of CBS can still be realized. Also, according to our simulations, ESPRIT typically yields better estimates for CBS in the coarray domain than root-MUSIC.

IV. CONVOLUTIONAL BEAMSPACE AND SPARSE RECOVERY

In this section, we show that CBS can also be used in conjunction with sparse signal recovery. In Section IV-A, we show how to integrate CBS into the basic single-snapshot sparse recovery problem, as depicted in Problem (52). In Section IV-B, we show that we can again use uniform decimation to reduce computational complexity as in Problem (54). In Section IV-C,

the multiple-snapshot version is also presented, as depicted in Problem (56) (without decimation) and Problem (57) (with decimation). The comparison of computational complexity between CBS and element-space is summarized in Section IV-D. As only the filter responses at discrete frequencies on the dictionary grid are relevant, the problem of designing discrete-frequency FIR filters is addressed in Section IV-E. Finally, some remarks are given in Section IV-F, and simulations are presented in Section IV-G.

Sparse signal representation techniques for DOA estimation have been studied in the literature [24]. In this context, a dictionary $\mathbf{D}$ of steering vectors $\mathbf{a}(\omega_i)$ on a grid of potential DOAs $\{\omega_i\}_{i=1}^d$ is considered, and the goal is to find a sparse signal $\mathbf{q} = [q_1\, q_2 \cdots q_d]^T$ that well represents the ULA output $\mathbf{x}$:

$$\mathbf{x} = \underbrace{[\mathbf{a}_N(\omega_1)\ \mathbf{a}_N(\omega_2)\ \cdots\ \mathbf{a}_N(\omega_d)]}_{\text{dictionary } \mathbf{D}} \mathbf{q} + \mathbf{e}, \tag{46}$$

where the error term $\mathbf{e}$ should be "small". The number of dictionary atoms d is typically much larger than D, the number of sources. A popular technique to obtain the sparse vector $\mathbf{q}$ is the Lasso method [48] that solves the following problem:

$$\min_{\mathbf{q}\in\mathbb{C}^d} \|\mathbf{q}\|_1 \tag{47a}$$

$$\text{subject to } \|\mathbf{x} - \mathbf{D}\mathbf{q}\|_2^2 \le \beta, \tag{47b}$$

where $\beta > 0$ is a parameter. The l_1-norm objective (47a) serves as a surrogate for sparsity, and the l_2-norm constraint (47b) limits the search space to where the noise term is small.

A. Convolutional Beamspace and Dictionaries

As in (3), we convolve the sequence $x(n), 0 \le n \le N-1$ with an FIR filter $h(n), 0 \le n \le L-1$ with $L < N$, and extract the steady state samples:

$$\mathbf{y} = \mathbf{H}\mathbf{x}. \tag{48}$$

As in (4), the response to a single DOA is (ignoring noise)

$$\mathbf{y} = \mathbf{H}\mathbf{a}_N(\omega) = e^{j(L-1)\omega} H(e^{j\omega}) \mathbf{a}_{N-L+1}(\omega). \tag{49}$$

Thus, (46) and (48) yield

$$\mathbf{y} = [\mathbf{a}_{N-L+1}(\omega_1)\ \cdots\ \mathbf{a}_{N-L+1}(\omega_d)]\, \mathbf{\Lambda}_h \mathbf{q} + \mathbf{H}\mathbf{e}, \tag{50}$$

where $\mathbf{\Lambda}_h$ is a diagonal matrix with ith diagonal element $(\mathbf{\Lambda}_h)_{ii} = e^{j(L-1)\omega_i} H(e^{j\omega_i})$. In other words, the diagonal elements are the frequency responses of $h(n)$ evaluated at the dictionary frequencies (with some phase shift). If $H(e^{j\omega})$ is a good narrowband lowpass filter, then

$$\mathbf{y} \approx \underbrace{[\mathbf{a}_{N-L+1}(\omega_1)\ \cdots\ \mathbf{a}_{N-L+1}(\omega_{d_0})]}_{\text{dictionary } \mathbf{D}_L} \mathbf{q}_0 + \mathbf{H}\mathbf{e}, \tag{51}$$

where $\omega_1, \omega_2, \ldots, \omega_{d_0}$ are the frequencies within the passband of $H(e^{j\omega})$, and $\mathbf{q}_0 \in \mathbb{C}^{d_0}$ is a significantly shorter vector than $\mathbf{q}$. Thus, a Lasso problem can be formulated for the CBS signal $\mathbf{y}$ as

$$\min_{\mathbf{q}_0\in\mathbb{C}^{d_0}} \|\mathbf{q}_0\|_1 \tag{52a}$$

$$\text{subject to } \|\mathbf{y} - \mathbf{D}_L\mathbf{q}_0\|_2^2 \le \beta. \tag{52b}$$

Here, the original dictionary $\mathbf{D}$ in (47b) is replaced by the dictionary $\mathbf{D}_L$ for CBS.

B. Decimation for Dictionaries

To reduce computational complexity by dimensionality reduction, we decimate the CBS signal $\mathbf{y}$ by M if $H(e^{j\omega})$ is a good filter with passband width $\approx 2\pi/M$. Let $v(n) = y(n + L - 1)$ so that $\mathbf{y} = [v(0)\ v(1) \cdots v(N-L)]^T$. Let $v_0(n) = v(Mn)$ and $\mathbf{v}_0 = [v_0(0)\ v_0(1)\ \cdots v_0(J_0 - 1)]^T$, where $J_0 = \lceil (N - L + 1)/M \rceil$, so the decimated version

$$\mathbf{v}_0 = [v(0)\ v(M)\ \cdots\ v((J_0-1)M)\ ]^T. \tag{53}$$

Then, we obtain the complexity-reduced problem

$$\min_{\mathbf{q}_0\in\mathbb{C}^{d_0}} \|\mathbf{q}_0\|_1 \tag{54a}$$

$$\text{subject to } \|\mathbf{v}_0 - \mathbf{D}_{L,0}\mathbf{q}_0\|_2^2 \le \beta, \tag{54b}$$

where $\mathbf{D}_{L,0}$ is the matrix obtained by retaining the rows $0, M, \ldots, (J_0-1)M$ of $\mathbf{D}_L$.

C. Multiple Snapshots for Dictionaries

The previous formulation is for a single snapshot. For multiple snapshots, we adopt the ℓ_1-SVD method proposed in [24]. Suppose we have K snapshots, $\mathbf{X} = [\mathbf{x}(1)\ \mathbf{x}(2) \cdots \mathbf{x}(K)]$. To reduce dimensionality, we take the SVD $\mathbf{X} = \mathbf{U}\mathbf{\Sigma}\mathbf{V}^H$ and retain a $N \times k$ matrix containing most of the signal power: $\mathbf{X}_{\rm SV} = \mathbf{U}\mathbf{\Sigma}\mathbf{J}_k = \mathbf{X}\mathbf{V}\mathbf{J}_k$, where $\mathbf{J}_k = [\mathbf{I}_k\ \mathbf{0}]^T$. We often take $k < K$ to be roughly the number of sources, and the original formulation of the ℓ_1-SVD method is then [24]

$$\min_{\mathbf{Q}\in\mathbb{C}^{d\times k}} \|\mathbf{Q}\|_{1,2} \tag{55a}$$

$$\text{subject to } \|\mathbf{X}_{\rm SV} - \mathbf{D}\mathbf{Q}\|_F^2 \le \beta, \tag{55b}$$

where $\|\mathbf{Q}\|_{1,2} = \sum_m \sqrt{\sum_n |\mathbf{Q}_{mn}|^2}$. That is, the ℓ_2-norm across singular vector samples is first computed for each spatial index, and then the ℓ_1-norm is computed across spatial samples for sparsity.

CBS can also be applied to the multiple snapshot scheme based on the ℓ_1-SVD method. We first convolve the spatial samples of each snapshot with a filter $h(n)$ of length L and extract the steady state samples: $\mathbf{Y} = \mathbf{H}\mathbf{X}$, similar to (48). Then, we take the SVD $\mathbf{Y} = \mathbf{U}_Y\mathbf{\Sigma}_Y\mathbf{V}_Y^H$ and retain a $(N - L + 1) \times k_0$ matrix containing most of the signal power: $\mathbf{Y}_{\rm SV} = \mathbf{U}_Y\mathbf{\Sigma}_Y\mathbf{J}_{k_0} = \mathbf{Y}\mathbf{V}_Y\mathbf{J}_{k_0}$. A multiple-snapshot version of Problem (52) can then be formulated as

$$\min_{\mathbf{Q}_0\in\mathbb{C}^{d_0\times k_0}} \|\mathbf{Q}_0\|_{1,2} \tag{56a}$$

$$\text{subject to } \|\mathbf{Y}_{\rm SV} - \mathbf{D}_L\mathbf{Q}_0\|_F^2 \le \beta. \tag{56b}$$

Likewise, a decimated version can be considered. Let $\mathbf{V}_0 = [\mathbf{v}_0(1)\ \mathbf{v}_0(2) \cdots \mathbf{v}_0(K)]$ be the multiple-snapshot counterpart of (53). Then, we take the SVD $\mathbf{V}_0 = \mathbf{U}_V\mathbf{\Sigma}_V\mathbf{V}_V^H$ and retain a $J_0 \times k_0$ matrix containing most of the signal power: $\mathbf{V}_{\rm SV} = \mathbf{U}_V\mathbf{\Sigma}_V\mathbf{J}_{k_0} = \mathbf{V}_0\mathbf{V}_V\mathbf{J}_{k_0}$. Then, a multiple-snapshot version of Problem (54) can be formulated as

$$\min_{\mathbf{Q}_0\in\mathbb{C}^{d_0\times k_0}} \|\mathbf{Q}_0\|_{1,2} \tag{57a}$$

$$\text{subject to } \|\mathbf{V}_{\rm SV} - \mathbf{D}_{L,0}\mathbf{Q}_0\|_F^2 \le \beta. \tag{57b}$$

Problem (57) is expected to yield better performance than Problem (55) because fewer DOAs are to be recovered in (57). This is indeed the case as we shall see in simulations.

TABLE IV
COMPARISON OF COMPUTATIONAL COMPLEXITY OF SPARSE RECOVERY METHODS

Algorithm	Number of optimization variables
Element-space (single snapshot)	d
Element-space ℓ_1-SVD (multiple-snapshot)	dk
CBS (single snapshot)	$d_0 \approx d/M$
CBS ℓ_1-SVD (multiple-snapshot)	$d_0 k_0 \approx dk/M^2$

TABLE V
RUNNING TIME PER MONTE CARLO RUN FOR DICTIONARY METHODS (FIG. 9) WHEN THERE ARE 10 OUT-OF-BAND DOAS

Algorithm	Running time (sec.)
CBS	0.458
Element-space	4.13

D. Computational Complexity

An important advantage of CBS is reduced computational complexity. The comparison of computational complexity between CBS and element-space is summarized in Table IV. Assume that the filter $H(e^{j\omega})$ used in CBS has passband width $\approx 2\pi/M$, and that the dictionary grid ω_i is a uniform grid of frequencies in $[0, 2\pi)$. Then, d in Problem (47a) and d_0 in Problems (52) and (54) are related by $d_0 \approx d/M$. That is, the number of optimization variables of CBS is only $1/M$ of that of element-space for the single-snapshot case.

Next, consider the multiple-snapshot case. According to [24], to get adequate performance, we have to take k to be roughly the number of sources D in Problem (55). As only the D_0 sources in the passband are effective after filtering, we can take $k_0 \approx D_0$ in Problem (56). If the sources are roughly uniformly distributed, then $D_0 \approx D/M$, so $k_0 \approx D/M$. Then, dk in Problem (55) and $d_0 k_0$ in Problems (56) and (57) are related by $d_0 k_0 \approx dk/M^2$. That is, the number of optimization variables of CBS is only $1/M^2$ of that of element-space for the multiple-snapshot case using the ℓ_1-SVD method. This can be a very significant complexity reduction. A direct comparison of running time for CBS and element-space is also presented in Table V.

E. Filters Designed for Dictionaries

An interesting question that arises for CBS dictionaries is how to design the filter $H(e^{j\omega})$. One can directly adopt standard methods such as the Parks-McClellan algorithm, the window method, and so on [28], but these standard filters are designed to be optimal or sub-optimal over continuous frequencies ω. The fact that only the response $H(e^{j\omega_i})$ at the *discrete* frequencies $\omega_i, i = 1, \ldots, d$ are relevant to CBS dictionaries, as in (50), can be leveraged to design better filters for dictionaries.

Consider a Type I [28], [32] linear-phase FIR filter $h(n), 0 \le n \le L-1$ such that L is odd and that $h(n)$ is even symmetric, i.e., $h(L-1-n) = h(n)$. Type I is just for illustration, and other types of linear-phase FIR filters can be designed similarly. It can be shown that $H(e^{j\omega}) = e^{-j\omega\frac{L-1}{2}} A(\omega)$, where $A(\omega) = \sum_{m=0}^{M} b_m \cos(m\omega)$ where $M = (L-1)/2$, $b_0 = h(M)$, and $b_m = 2h(M-m)$ otherwise. Note that $|A(\omega)|$ is the magnitude response. Then, a standard *minimax* filter design problem can be formulated as [28]

$$\min_{h(\frac{L-1}{2}),\ldots,h(L-1)} \max_{\omega\in\Omega_p\cup\Omega_s} |W(\omega)(A(\omega) - A_d(\omega))|, \quad (58)$$

where Ω_p is the passband, Ω_s is the stopband,

$$A_d(\omega) = \begin{cases} 1, & \omega \in \Omega_p \\ 0, & \omega \in \Omega_s \end{cases} \quad (59)$$

is the desired magnitude response, and $W(\omega)$ is a weighting function such that

$$W(\omega) = \begin{cases} 1, & \omega \in \Omega_p \\ \lambda, & \omega \in \Omega_s \end{cases} \quad (60)$$

for some design parameter $\lambda > 0$. Note that $W(\omega)(A(\omega) - A_d(\omega))$ is affine in the variables $h(\frac{L-1}{2}), \ldots, h(L-1)$, and that the absolute function is a convex function. Hence, since the composition of a convex function with an affine mapping is still convex, $|W(\omega)(A(\omega) - A_d(\omega))|$ is convex. Moreover, the pointwise supremum of a collection of convex functions is still convex, so we conclude that Problem (58) is a convex problem. Traditionally, the passband Ω_p and stopband Ω_s are continuous. However, as described earlier, only the frequency response $H(e^{j\omega_i})$ at the discrete frequency grid $\{\omega_i\}_{i=1}^d$ are relevant, so instead of (58), we can consider

$$\min_{h(\frac{L-1}{2}),\ldots,h(L-1)} \max_{\omega\in\Omega_p'\cup\Omega_s'} |W(\omega)(A(\omega) - A_d(\omega))|, \quad (61)$$

where $\Omega_p' = \{\omega_i, 1 \le i \le d \mid \omega_i \in \Omega_p\}$ and $\Omega_s' = \{\omega_i, 1 \le i \le d \mid \omega_i \in \Omega_s\}$. We may also choose a sparser frequency grid (e.g., only include even i's) for Problem (61) to obtain a potentially better filter. See Fig. 10(a) for an example. Problem (61) can be readily solved by any numerical convex program solver such as `CVX` [49]. Such a filter should have a better response than a standard filter in the literature (e.g., `firpm` of MATLAB) over the discrete frequencies $\omega_1, \ldots, \omega_d$.

F. Remarks

1) The choice of the grid of potential DOAs $\{\omega_i\}_{i=1}^d$ is in the designer's hands. One way is to choose a *uniform* grid in ω. Another is to choose a grid uniform in the physical DOA θ. Recall that $\omega = \pi \sin\theta$. Hence, the second way leads to a *nonuniform* grid in ω, with denser points in high-frequency part and sparser points in low-frequency part. It is hard to say which type, uniform or nonuniform, is better because it depends on the actual locations of the DOAs. Yet, if the DOAs are expected to be uniformly distributed over the physical angle θ, it makes sense to choose the nonuniform type. An interesting observation is that the type of the grid also affects the result of filter design. For example, suppose we want to design a lowpass filter $H(e^{j\omega})$. If we choose the nonuniform type of grid, with denser points in high-frequency part, then the resulting filter will have better attenuation for the high-frequency stopband. That is, the density

of the grid points induces a weighting effect across different frequency bands. See Fig. 11 for a numerical demonstration.

2) Instead of using a filter $H(e^{j\omega})$, we can use a filter bank $H_i(e^{j\omega}), 0 \le i \le M-1$ to cover the full range $0 \le \omega < 2\pi$ as in Fig. 3. Using these, we obtain the CBS signals $\mathbf{y}_i, 0 \le i \le M-1$. Solving an optimization problem as in (52) for each $\mathbf{y}_i$ in parallel reveals the D_i DOAs falling into the ith subband. The union of these DOAs gives the set of all D DOAs. Similar idea can be applied to Problems (54), (56), and (57). Note that here we do not confine each filter $H_i(e^{j\omega})$ to be a spectral factor of a Nyquist filter as we did for subspace-based methods such as MUSIC because the property that the noise is white is not used in sparse signal recovery.

3) One method for selecting the parameter β in the sparse recovery problems (e.g., Problem (47a)) was proposed in [24]. The method is based on estimating the variance of the left hand side of the constraint (e.g., $\|\mathbf{x}-\mathbf{D}\mathbf{q}\|_2^2$ in (47b)). It was originally proposed for element-space, but we can extend the method to CBS. In the simulations, we will follow this method to choose β.

G. Simulations

Unlike in subspace-based methods such as MUSIC, where we estimate the number of DOAs and their locations separately, for dictionaries, we estimate them together. Specifically, for element-space, after getting the optimal solution $\hat{\mathbf{Q}}$ for Problem (55), we plot the *dictionary power spectrum* $P(\omega_i) = \sum_n |\hat{\mathbf{Q}}_{in}|^2$ for $1 \le i \le d$. Then, we declare that there is a source at ω_i if there is a peak (local maximum) that is larger than a particular threshold: $P(\omega_i) \ge \epsilon$. The same method is used for CBS. See Fig. 9(a)–(b) for an example (described below). In all examples, we use $\lambda = 1$ in (60).

We first compare the most complexity-reduced version of CBS (57) with the element-space (55) under multiple snapshots. Consider a ULA with $N = 99$ sensors. First assume a Parks-McClellan filter $H(z)$ of length $L = 16$ and with cutoff π/M is used, where $M = 4$ is the decimation ratio. A dictionary of 200 points uniform in ω is used. There are two in-band DOAs at angles -0.573° and 0.573°, which are exactly on the grid of the dictionary for simplicity. We vary the number of out-of-band DOAs, while they are uniformly placed in the range $\omega \in [0.5\pi, 0.98\pi]$. The reduced dimension for the ℓ_1-SVD method in (55) and (57) is chosen as $k = k_0 = 3$. The peak threshold $\epsilon = 0.1$ is used (with the spectrum normalized to have a maximum value 1). We choose $\beta = 641.7$ in (55b) and $\beta = 221.7$ in (57b) according to the method in [24], as described in Remark 3 above. Fig. 9(a) shows the probability of resolving the correct number of in-band DOAs. We use $K = 100$ snapshots and 100 Monte Carlo runs to get the plot. As the number of out-of-band DOAs increases, the probability of resolution decreases significantly for element-space, while the probability of resolution is always one for CBS due to good stopband attenuation. Note that there is a trade-off between the performance and the reduced dimension k for the ℓ_1-SVD method for element-space. A large k can lead to better performance, but it requires higher computational complexity. Typical dictionary power spectra of CBS and element-space for a Monte Carlo run with 10 out-of-band DOAs are shown in Fig. 9(b)–(c). For CBS, only the passband part is plotted. The two in-band DOAs are clearly distinguished by CBS, but they cannot be resolved by element-space. The running time

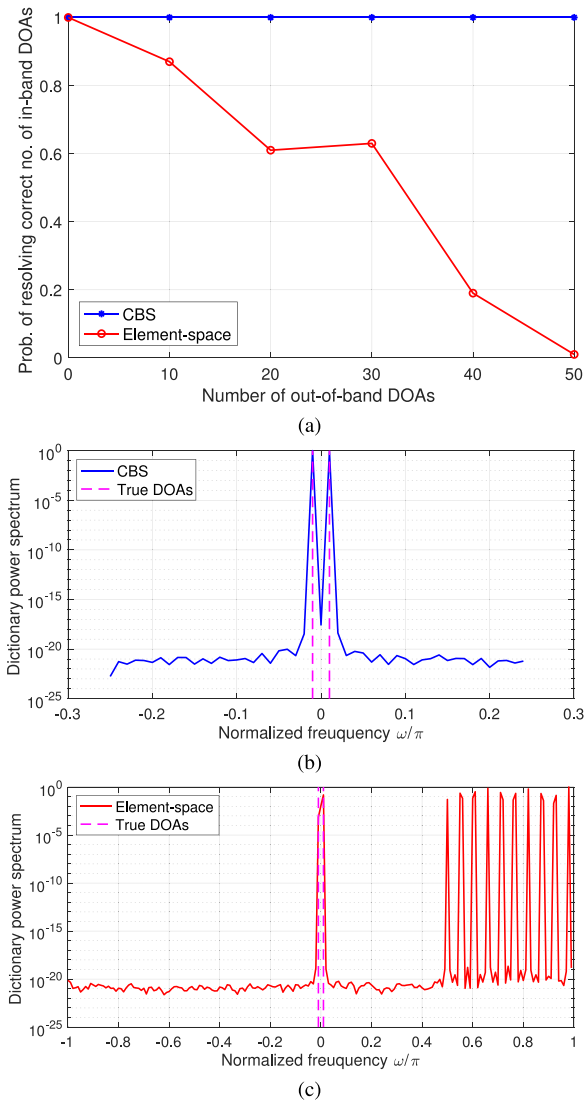

Fig. 9. Performance of CBS and element-space dictionaries when there are many out-of-band DOAs. (a) Probability of resolution. (b) Typical dictionary power spectrum of CBS. (c) Typical dictionary power spectrum of element-space.

per Monte Carlo run for CBS and element-space is shown in Table V. The computational complexity of CBS is about 9 times lower than that of element-space.

Next, the impact of a well-designed *minimax-discrete* type filter described in Section IV-E (instead of the Parks-McClellan filter) is studied. Consider a ULA with $N = 99$ sensors. Problem (57) is to be solved again. A dictionary of 200 points uniform in ω is used. We compare lowpass FIR filters with length $L = 16$ designed using the Parks-McClellan algorithm [28] and our minimax-discrete optimization problem (61). The passband is $\Omega_p = [0, 0.1\pi]$, and the stopband is $\Omega_s = [0.4\pi, \pi]$. For the filter design problem (61), we use a grid of 50 points uniform in ω, which is sparser than the dictionary grid. Two in-band DOAs are at angles $-0.6^\circ, 0.6^\circ$ with equal powers $p_k = 1$, and 10 out-of-band DOAs are uniformly placed in the range $\omega \in [0.5\pi, 0.98\pi]$ with varying equal powers. Here all the DOAs are not on the dictionary grid, in contrast to the previous example. The decimation ratio is $M = 4$. The reduced dimension for the ℓ_1-SVD method is chosen as $k_0 = 2$. The same peak threshold

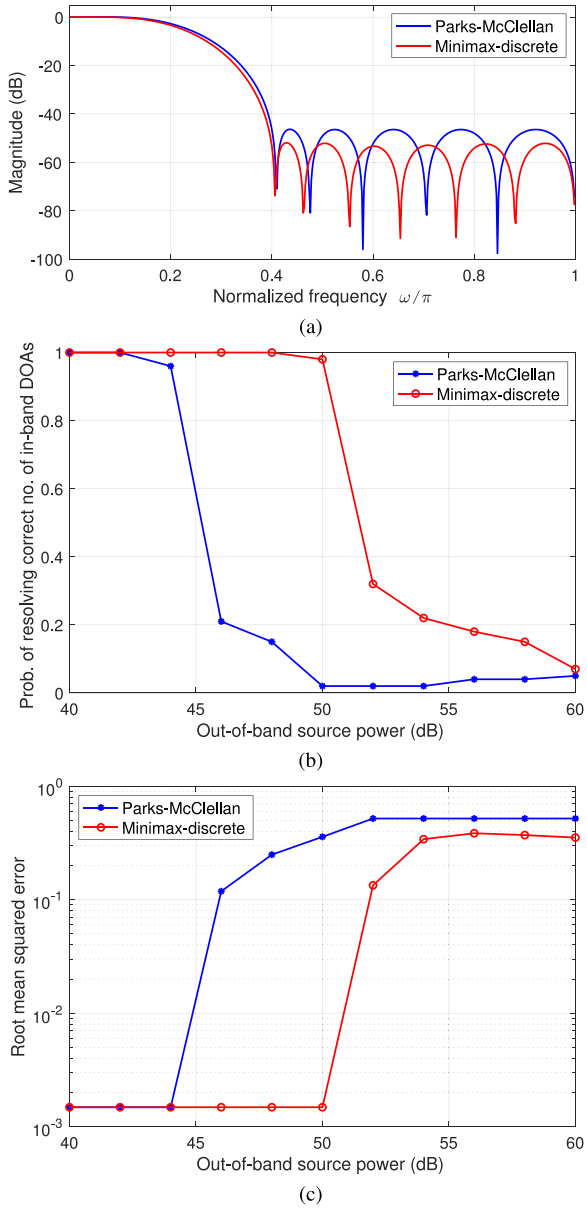

Fig. 10. Performance of minimax-discrete and Parks-McClellan filters for CBS dictionaries when there are powerful out-of-band sources. (a) Filter responses. (b) Probability of resolution. (c) RMSE.

$\epsilon = 0.1$ is used, and we choose $\beta = 1338$ in (57b) according to the method in [24], as described in Remark 3 in Section IV-F. In Fig. 10(a), the magnitude responses of the filters are plotted. Although the minimax-discrete type filter is optimized only over a discrete grid, it has better attenuation over the whole continuous stopband. We experimentally found that if we use a grid of 200 rather than 50 points for filter design, the resulting minimax-discrete filter is almost the same as the Park-McClellan filter. This is expected because the denser the grid, the closer the discrete type to the continuous type. Due to the better stopband attenuation, as we vary the power of the out-of-band sources, the minimax-discrete filter has larger probability of resolving the correct number of in-band DOAs and smaller RMSE in detected in-band source angles, as shown in Fig. 10(b)–(c). Here we use $K = 100$ snapshots and 100 Monte Carlo runs. Due to the powerful out-of-band DOAs, element-space always has

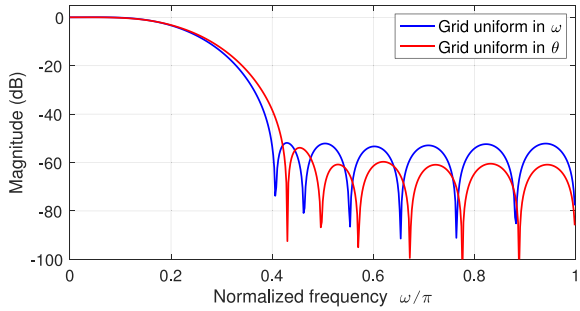

Fig. 11. Responses of minimax-discrete filters designed based on different types of grids.

zero probability of resolution, so is not plotted in Fig. 10. For smaller out-of-band source power in Fig. 10(c), the minimum possible RMSE ($\approx 10^{-3}$), which is the distance between each true DOA and the closest grid point, is achieved. This example shows that designing discrete-frequency filters specifically for CBS dictionaries makes a difference.

Finally, Fig. 11 shows how the design result of minimax-discrete type filers is affected by the type of grid. The filter length is $L = 16$. The passband is $\Omega_p = [0, 0.1\pi]$, and the stopband is $\Omega_s = [0.4\pi, \pi]$. Grids of 50 points uniform in ω and uniform in θ are compared. Due to the denser grid points in high frequencies, the latter has a better attenuation in the high-frequency range at the expense of a worse response around the transition band. Hence, if there are powerful out-of-band sources far from the transition band, the latter is better, but if they are near the transition band, the former is better.

V. Conclusion

In this paper we introduced the convolutional beamspace (CBS) as an alternative to classical beamspace methods of array processing. While enjoying the computational advantages of classical beamspace, CBS also allows the direct use of root-MUSIC and ESPRIT without any complicated preprocessing. A simple error analysis showed that CBS can have better estimation performance when the sources are correlated. We also developed CBS methods for coarrays of sparse arrays, and for dictionary based methods which use dictionaries of steering vectors to obtain sparse representations of array data. Due to dimension reduction and effective filtering of out-of-band sources, many advantages are obtained across all these frameworks, such as lower computational complexity, better DOA estimates, and improved resolution.

References

[1] G. Bienvenu and L. Kopp, "Decreasing high resolution method sensitivity by conventional beamformer preprocessing," in *Proc. IEEE Int. Conf. Acoust., Speech, Signal Process.*, Mar. 1984, pp. 714–717.

[2] B. Van Veen and B. Williams, "Structured covariance matrices and dimensionality reduction in array processing," in *Proc. 4th Annu. ASSP Workshop Spec. Est. Model.*, 1988, pp. 168–171.

[3] K. M. Buckley and X. L. Xu, "Reduced-dimension beam-space broad-band source localization: Preprocessor design," in *Proc. SPIE, Adv. Algorithms Architectures Signal Process. III*, Feb. 1988, pp. 368–376.

[4] H. B. Lee and M. S. Wengrovitz, "Improved high-resolution direction-finding through use of homogeneous constraints," in *Proc. 4th Annu. ASSP Workshop Spec. Est. Model.*, Aug. 1988, pp. 152–157.

[5] H. L. Van Trees, *Optimum Array Processing*. Wiley New York, 2002.

[6] Z. Guo, X. Wang, and W. Heng, "Millimeter-wave channel estimation based on 2-D beamspace MUSIC method," *IEEE Trans. Wireless Commun.*, vol. 16, no. 8, pp. 5384–5394, Aug. 2017.
[7] R. Yang, D. Gray, and W. Al-Ashwal, "Estimation of the DOAs of coherent signals in beam space processing for phased arrays," in *Proc. IEEE Int. Conf. Radar*, Aug. 2018, pp. 1–5.
[8] H. Zhao, N. Zhang, and Y. Shen, "Robust beamspace design for direct localization," in *Proc. IEEE Int. Conf. Acoust., Speech Signal Process.*, May 2019, pp. 4360–4364.
[9] R. Schmidt, "Multiple emitter location and signal parameter estimation," *IEEE Trans. Antennas Propag.*, vol. 34, no. 3, pp. 276–280, Mar. 1986.
[10] B. D. Rao and K. V. S. Hari, "Performance analysis of Root-Music," *IEEE Trans. Acoust., Speech, Signal Process.*, vol. 37, no. 12, pp. 1939–1949, 1989.
[11] R. Roy and T. Kailath, "ESPRIT – estimation of signal parameters via rotational invariance techniques," *IEEE Trans. Acoust., Speech, Signal Process.*, vol. 37, no. 7, pp. 984–995, Jul. 1989.
[12] H. B. Lee and M. S. Wengrovitz, "Resolution threshold of beamspace MUSIC for two closely spaced emitters," *IEEE Trans. Acoust., Speech, Signal Process.*, vol. 38, no. 9, pp. 1545–1559, Sep. 1990.
[13] X. L. Xu and K. M. Buckley, "Statistical performance comparison of MUSIC in element-space and beam-space," in *Proc. IEEE Int. Conf. Acoust., Speech, Signal Process.*, 1989, pp. 2124–2127.
[14] M. D. Zoltowski, G. M. Kautz, and S. D. Silverstein, "Beamspace root-MUSIC," *IEEE Trans. Signal Process.*, vol. 41, no. 1, pp. 344–364, Jan. 1993.
[15] G. Xu, S. D. Silverstein, R. H. Roy, and T. Kailath, "Beamspace ESPRIT," *IEEE Trans. Signal Process.*, vol. 42, no. 2, pp. 349–356, Feb. 1994.
[16] A. L. Swindlehurst, E. Ayanoglu, P. Heydari, and F. Capolino, "Millimeter-wave massive MIMO: The next wireless revolution?," *IEEE Commun. Mag.*, vol. 52, no. 9, pp. 56–62, Sep. 2014.
[17] X. Gao, L. Dai, and A. M. Sayeed, "Low RF-complexity technologies to enable millimeter-wave MIMO with large antenna array for 5G wireless communications," *IEEE Commun. Mag.*, vol. 56, no. 4, pp. 211–217, Apr. 2018.
[18] P. Stoica and A. Nehorai, "MUSIC, maximum likelihood, and Cramer-Rao bound," *IEEE Trans. Acoust., Speech, Signal Process.*, vol. 37, no. 5, pp. 720–741, May 1989.
[19] A. T. Moffet, "Minimum-redundancy linear arrays," *IEEE Trans. Antennas Propag.*, vol. 16, no. 2, pp. 172–175, Mar. 1968.
[20] P. Pal and P. P. Vaidyanathan, "Nested arrays: A novel approach to array processing with enhanced degrees of freedom," *IEEE Trans. Signal Process.*, vol. 58, no. 8, pp. 4167–4181, Aug. 2010.
[21] P. P. Vaidyanathan and P. Pal, "Sparse sensing with co-prime samplers and arrays," *IEEE Trans. Signal Process.*, vol. 59, no. 2, pp. 573–586, Feb. 2011.
[22] C.-L. Liu and P. P. Vaidyanathan, "Super nested arrays: Linear sparse arrays with reduced mutual coupling–Part I: Fundamentals," *IEEE Trans. Signal Process.*, vol. 64, no. 15, pp. 3997–4012, Aug. 2016.
[23] S. Qin, Y. D. Zhang, and M. G. Amin, "Generalized coprime array configurations for direction-of-arrival estimation," *IEEE Trans. Signal Process.*, vol. 63, no. 6, pp. 1377–1390, Mar. 2015.
[24] D. Malioutov, M. Cetin, and A. S. Willsky, "A sparse signal reconstruction perspective for source localization with sensor arrays," *IEEE Trans. Signal Process.*, vol. 53, no. 8, pp. 3010–3022, Aug. 2005.
[25] S. D. Silverstein, W. E. Engeler, and J. A. Tardif, "Parallel architectures for multirate superresolution spectrum analyzers," *IEEE Trans. Circuits Syst.*, vol. 38, no. 4, pp. 449–453, Apr. 1991.
[26] A. Tkacenko and P. P. Vaidyanathan, "The role of filter banks in sinusoidal frequency estimation," *J. Franklin Inst.*, vol. 338, no. 5, pp. 517–547, 2001.
[27] L. Qiu, Y. Cai, R. C. de Lamare, and M. Zhao, "Reduced-rank DOA estimation algorithms based on alternating low-rank decomposition," *IEEE Signal Process. Lett.*, vol. 23, no. 5, pp. 565–569, 2016.
[28] A. V. Oppenheim and R. W. Schafer, *Discrete-time Signal Processing*. Prentice Hall, 2010.
[29] L. Wang, R. C. de Lamare, and M. Haardt, "Direction finding algorithms based on joint iterative subspace optimization," *IEEE Trans. Aerosp. Electron. Syst.*, vol. 50, no. 4, pp. 2541–2553, 2014.
[30] R. C. de Lamare and R. Sampaio-Neto, "Adaptive reduced-rank processing based on joint and iterative interpolation, decimation, and filtering," *IEEE Trans. Signal Process.*, vol. 57, no. 7, pp. 2503–2514, 2009.
[31] P. P. Vaidyanathan and P.-C. Chen, "Convolutional beamspace for array signal processing," in *Proc. IEEE Int. Conf. Acoust., Speech, Signal Process.*, 2020.
[32] P. P. Vaidyanathan, *Multirate Systems and Filter Banks*. Prentice Hall, Englewood Cliffs, N.J., 1993.
[33] J. G. Proakis, *Digital Communications*. Mc-Graw Hill, New York, 2008.
[34] H. Samueli, "On the design of optimal equiripple FIR digital filters for data transmission applications," *IEEE Trans. Circuits Syst.*, vol. 35, no. 12, pp. 1542–1546, Dec. 1988.
[35] P. P. Vaidyanathan, T. Q. Nguyen, Z. Doganata, and T. Saramaki, "Improved technique for design of perfect reconstruction FIR QMF banks with lossless polyphase matrices," *IEEE Trans. Acoust., Speech, Signal Process.*, vol. 37, no. 7, pp. 1042–1056, Jul. 1989.
[36] P. P. Vaidyanathan and T. Q. Nguyen, "Eigenfilters: A new approach to least-squares FIR filter design and applications including Nyquist filters," *IEEE Trans. Circuits Syst.*, vol. 34, no. 1, pp. 11–23, Jan. 1987.
[37] H. Samueli, "On the design of FIR digital data transmission filters with arbitrary magnitude specifications," *IEEE Trans. Circuits Syst.*, vol. 38, no. 12, pp. 1563–1567, Dec. 1991.
[38] R. D. Koilpillai and P. P. Vaidyanathan, "Cosine-modulated FIR filter banks satisfying perfect reconstruction," *IEEE Trans. Signal Process.*, vol. 40, no. 4, pp. 770–783, Apr. 1992.
[39] Y.-P. Lin and P. P. Vaidyanathan, "A Kaiser window approach for the design of prototype filters of cosine modulated filterbanks," *IEEE Signal Process. Lett.*, vol. 5, no. 6, pp. 132–134, Jun. 1998.
[40] P. P. Vaidyanathan and P.-Q. Hoang, "Lattice structures for optimal design and robust implementation of two-channel perfect-reconstruction QMF banks," *IEEE Trans. Acoust., Speech, Signal Process.*, vol. 36, no. 1, pp. 81–94, Jan. 1988.
[41] M. Vetterli and J. Kovacevic, *Wavelets and Subband Coding*. Prentice Hall, Englewood Cliffs, N.J., 1995.
[42] P. Stoica and A. Nehorai, "Comparative performance study of element-space and beam-space MUSIC estimators," *Circuits, Syst. Signal Process.*, vol. 10, no. 3, pp. 285–292, Sep. 1991.
[43] A. J. Weiss and B. Friedlander, "Preprocessing for direction finding with minimal variance degradation," *IEEE Trans. Signal Process.*, vol. 42, no. 6, pp. 1478–1485, 1994.
[44] P. Stoica and A. Nehorai, "Performance study of conditional and unconditional direction-of-arrival estimation," *IEEE Trans. Acoust., Speech, Signal Process.*, vol. 38, no. 10, pp. 1783–1795, Oct. 1990.
[45] Tie-Jun Shan, M. Wax, and T. Kailath, "On spatial smoothing for direction-of-arrival estimation of coherent signals," *IEEE Trans. Acoust., Speech, Signal Process.*, vol. 33, no. 4, pp. 806–811, 1985.
[46] M. D. Zoltowski, S. D. Silverstein, and C. P. Mathews, "Beamspace root-MUSIC for minimum redundancy linear arrays," *IEEE Trans. Signal Process.*, vol. 41, no. 7, pp. 2502–2507, Jul. 1993.
[47] C.-L. Liu and P. P. Vaidyanathan, "Remarks on the spatial smoothing step in coarray MUSIC," *IEEE Signal Process. Lett.*, vol. 22, no. 9, pp. 1438–1442, Sep. 2015.
[48] R. Tibshirani, "Regression shrinkage and selection via the lasso," *J. Roy. Stat. Soc.: Series B (Methodological)*, vol. 58, no. 1, pp. 267–288, 1996.
[49] M. Grant and S. Boyd, "CVX: Matlab software for disciplined convex programming, version 2.1," https://cvxr.com/cvx, Mar. 2014.

Po-Chih Chen (Student Member, IEEE) was born in 1993. He received the B.S. and M.S. degrees in electrical engineering and communication engineering from National Taiwan University, Taipei, Taiwan, in 2015 and 2017, respectively. He is currently working toward the Ph.D. degree in electrical engineering with the California Institute of Technology, Pasadena, CA. His research interests are in signal processing, array processing, sparse arrays, and distributed algorithms for arrays.

P. P. Vaidyanathan (Life Fellow, IEEE) received the B.Sc., B.Tech. and M.Tech. degrees from the University of Calcutta, India, in 1974, 1977 and 1979, respectively, and the Ph.D. degree in electrical and computer engineering from the University of California at Santa Barbara, in 1982. He is the Kiyo and Eiko Tomiyasu Professor of electrical engineering with the California Institute of Technology, (Caltech). He was the recipient of the IEEE CAS Society Golden Jubilee Medal, the Terman Award of the ASEE, the IEEE Gustav Robert Kirchhoff Technical Field Award in 2016, and the IEEE Signal Processing Society's Technical Achievement Award in 2002, Education Award in 2012, and Society Award in 2016. He was also the recipient of multiple awards for teaching at Caltech, including the Northrop Grumman teaching prize. He is a member of the U.S. National Academy of Engineering.